

Evolution of the North Anatolian Fault from a diffuse to a localized shear zone in the North Aegean Sea during the Plio-Pleistocene

M. Rodriguez,¹ D. Sakellariou,² C. Gorini,³ A. Janin,¹ E. D'Acremont,³ L. Le Pourhiet^{1,3},
 N. Chamot-Rooke,¹ K. Tsampouraki-Kraounaki,² I. Morfis,² G. Rousakis,² P. Henry,⁴
 A. Lurin,¹ M. Delescluse,¹ P. Briole^{1,5}, A. Rigo,¹ S. Arsenikos,⁵ C. Bulois,¹
 D. Fernández-Blanco,⁶ A. Beniést,⁷ C. Grall,⁸ F. Chanier,⁹ F. Caroir,⁹ J-X. Dessa,¹⁰
 D. Oregioni¹⁰ and A. Necessian¹¹

¹Laboratoire de Géologie, Ecole normale supérieure, PSL Research University, CNRS UMR 8538, 24 rue Lhomond, 75005 Paris, France.

E-mail: rodriguez@geologie.ens.fr

²Institute of Oceanography, Hellenic Center of Marine Research, GR-19013 Anavyssos, Greece

³Sorbonne Université, UPMC Université Paris 06, UMR 7193, IStEP, F-75005 Paris, France

⁴Centre Européen de Recherche Et d'Enseignement Des Géosciences de L'Environnement, Aix-Marseille Université, Marseille 13545, France

⁵Beicip-Franlab, Rueil-Malmaison 78532, France

⁶Barcelona Center for Subsurface Imaging, Instituto de Ciencias del Mar, CSIC, Barcelona 08028, Spain

⁷Department of Earth Sciences, Vrije Universiteit Amsterdam, Amsterdam 1081 HV, the Netherlands

⁸LIENSs, La Rochelle University, UMR 7266, Olympe de Gouges, 17000 La Rochelle, France

⁹Univ. Lille, CNRS, Univ. Littoral Côte d'Opale, UMR 8187, LOG, Laboratoire d'Océanologie et de Géosciences, F59000 Lille, France

¹⁰Géoazur, Université de Nice-Sophia Antipolis-CNRS-OCA, UMR 7329, Valbonne 06560, France

¹¹Institut de physique du globe de Paris, Université de Paris, CNRS, Paris F-75005, France

Accepted 2023 September 12. Received 2023 August 28; in original form 2023 March 4

SUMMARY

The North Anatolian Fault is the ~1200-km-long active continental transform boundary between Anatolia and Eurasia. This strike-slip system initiated around 10–12 Ma and experienced diachronous episodes of strain localization along its strike. The structural evolution of the ~350-km-long fault segments crossing the North Aegean Sea remains to be accurately investigated. There, the modern North Anatolian Fault is localized along two main branches: the northern branch ends at the North Aegean Trough and the southern branch ends at the Edremit-Skyros Trough. The Evia Basin is located in the North Aegean Domain between the North Anatolian Fault and the Corinth Rift. This study presents seismic reflection lines crossing the aforementioned structures of the North Aegean Domain, which document their subsurface structure and the sedimentary record of their activity since the Messinian. The seismic-reflection data set is tied to regional-scale stratigraphic markers, which constrains the age of main tectonic events related to the formation of the North Anatolian Fault. The seismic-reflection lines show that the two main branches of the North Anatolian Fault became localized structures at 1.3–2 Ma, coevally with the formation of the Evia Basin. Since 2 Ma, the North Aegean Troughs developed as a series of horsetail basins propagating westwards at the termination of the branches of the North Anatolian Fault. On a regional scale, the wide and diffuse North Anatolian transtensive shear zone active from Serravalian to Late Pliocene turned into a narrower shear zone at the two main branches of the North Anatolian Fault since the Early Pleistocene. This abrupt episode of strain localization occurred in the frame of the major Early Pleistocene change in stress regime from NE–SW to N–S extension, which has been observed throughout the Aegean Sea.

Key words: Continental tectonics; strike-slip and transform; Submarine Tectonics and volcanism; Transform faults.

1 INTRODUCTION

Transform faults are major lithospheric-scale tectonic structures acting as plate boundaries (Woodcock & Daly 1986; Mann 2007), along which relative plate motion occurs horizontally along the fault's strike. The accumulated relative plate motion along transform boundaries juxtaposes sections of the lithosphere with different histories, ages and hence, mechanical properties (Ben Zion & Sammis 2003). The complex rheology of the continental domain results in both localized (e.g. the Dead Sea Fault; Garfunkel & Ben-Avraham 1996) and diffuse continental transform systems (e.g. the Trans-Alboran Shear Zone; Lafosse *et al.* 2020). Some transform systems have also been shown to alternate localized and diffuse strain along their strike (e.g. the San Andreas Fault; Wesnousky 2005; and the North Anatolian Fault; Sengör *et al.* 2019).

Field studies reveal that continental transforms initiate as several hundreds of kilometres-wide distributed areas of deformation, forming a shear zone that is composed of scattered oblique en-échelon strands (Tchalenko & Ambraseys 1970; Sengör *et al.* 2005, 2014; Wesnousky 2005; Mann 2007). During fault initiation, motion is distributed over several individual fault segments. As finite relative motion increases, fault strands progressively connect into continuous and localized strike-slip fault segments. The increased connection of fault strands shapes narrower shear zones (<100 km wide) with local structural complexities in stepover (releasing or restraining bends). The localization of strike-slip segments leaves some initial oblique strands deactivated. The timing of strain localization within the wide shear zone may differ from one fault segment to another. The lifetime of such shear systems in the continental setting is in the order of 10^7 yr (Sengör *et al.* 2019). Analogue models reproduce the transition from an initial diffuse shear zone composed of Riedel faults to a localized fault formed by the linkage of shear segments (Tchalenko 1970; Dooley & Schreurs 2012; Lefevre *et al.* 2020).

The North Anatolian Fault system, located in the Eastern Mediterranean domain (Figs 1 and 2), is the 1200-km-long dextral strike-slip boundary between the Anatolian and Eurasian tectonic plates (Figs 1 and 2), which connects the Anatolia–Arabia–Eurasia triple junction in the East (Hubert Ferrari *et al.* 2010) to the Hellenic Subduction Zone (Flerit *et al.* 2004; Ferentinos *et al.* 2018; Sakellariou & Tsampouraki-Kraounaki 2018; Sakellariou *et al.* 2018). The North Anatolian Fault triggers frequent earthquakes above $M_w \sim 7$ (e.g. Izmit and Duzce events in 1999; Hubert-Ferrari *et al.* 2000; Bulut *et al.* 2018) and its submarine segments are a potential source of tsunamis (Hébert *et al.* 2005; Reicherter *et al.* 2010; Janin *et al.* 2019).

The North Anatolian Fault transects continental lithosphere with significant along-strike strength variations, inherited from the successive geological events that shaped the Hellenides mountain belt prior to its collapse. As such, the North Anatolian Fault is a relevant case-study of a post-orogenic transform fault (Le Pourhiet *et al.* 2014; Jolivet *et al.* 2021).

The objective of this study is to constrain the structural evolution of the ~ 350 -km-long segment of the North Anatolian Fault crossing the North Aegean Sea (Figs 3 and 4), on the basis of a set of multibeam data (Ypother cruises, 2013–2016; Sakellariou *et al.* 2018) and seismic-reflection profiles (NAFAS cruise, 2017; Rodríguez *et al.* 2018; vintage seismic lines published in Beniest *et al.* 2016).

The present data set covers some of the major tectonic structures encountered in the North Aegean Domain, namely the North Aegean Trough, the Edremit-Skyros Trough and the Evia Basin (Figs 2–4).

There, the different steps of formation of the North Anatolian Fault remained poorly constrained due to the lack of seismic-reflection and stratigraphic data (Krijgsman *et al.* 2022). We define some regional stratigraphic markers for the period spanning the Messinian to the present-day (Laigle *et al.* 2000; Beniest *et al.* 2016; Ferentinos *et al.* 2018) to reach a precision in the ages of tectonic events comparable to the segments of the North Anatolian Fault observed in the Marmara Sea (Le Pichon *et al.* 2014). Finally, we provide structural maps of the post-Messinian evolution of the North Aegean Domain, from the Yeniçaga Fork east of Marmara to the Evia Basin in Greece (Fig. 2). Overall, our structural reconstructions of the North Anatolian Fault document the strain localization within a post-orogenic continental shear zone and the time of effective formation of such tectonic plates.

2 GEOLOGICAL BACKGROUND

2.1 Present-day configuration of the North Anatolian Fault in the North Aegean domain

The North Anatolian Fault is the plate boundary between Anatolia and Eurasia, with a current dextral strike-slip rate of 23 mm yr^{-1} (Le Pichon *et al.* 2003; Reilinger *et al.* 2006; Le Pichon & Kreemer 2010; Pérouse *et al.* 2012; Müller *et al.* 2013). The finite amount of dextral motion along the North Anatolian Fault is estimated to 85 ± 5 km, with some ambiguities in areas where slip is distributed over several fault strands (Sengör *et al.* 2005). The finite offset results from strike-slip rates that grew from $\sim 3 \text{ mm yr}^{-1}$ in the earliest stages of formation of the fault system to near-current slip rates since the Early Pleistocene (Hubert Ferrari *et al.* 2010).

In this study, the North Aegean Domain is defined as the area bounded to the south by the North Cycladic Detachment System, to the north by the Rhodope Detachment System, to the west by the Vardar Suture Zone and to the East by the Yeniçaga fork (Figs 1 and 2). The total amount of slip-rate along the North Anatolian Fault is accommodated by its northern and southern branches in the North Aegean Domain (Figs 1 and 2; Le Pichon *et al.* 2003).

The northern branch of the North Anatolian Fault crosses the Marmara Sea (i.e. the Main Marmara Fault; Le Pichon *et al.* 2001), then runs along the Gelibolu Peninsula and the Gulf of Saros until it connects the North Aegean Trough (Fig. 2). The North Anatolian Fault makes a $\sim 30^\circ$ bend at the connection between the Saros Gulf and the North Aegean Trough (Roussos & Lyssimachou 1991; Koukouvelas & Aydin 2002). The strike-slip rate of relative motion along the northern branch decreases from 21.2 mm yr^{-1} at the Gulf of Saros to $\sim 5 \text{ mm yr}^{-1}$ at the Sporadhes archipelago (Müller *et al.* 2013).

The southern branch of the North Anatolian Fault crosses the Biga Peninsula and connects the Edremit-Skyros Trough in the Aegean Sea (Fig. 2). The strain distribution of the southern branch of the North Anatolian Fault (Figs 2–4) is diffuse onland in Turkey (Sümer *et al.* 2018), whereas it is expressed as a localized structure offshore (Papanikolaou *et al.* 2019). The strike-slip rate along the southern branch is on the order of 10 mm yr^{-1} (Müller *et al.* 2013).

Both the North Aegean and the Edremit-Skyros Troughs reveal horsetail structures (Figs 3 and 4). Horsetail structures are commonly observed at the termination of strike-slip faults (Basile & Brun 1999): they consist in numerous oblique splays rooting on the main strike-slip faults and isolating a series of transtensive basins.

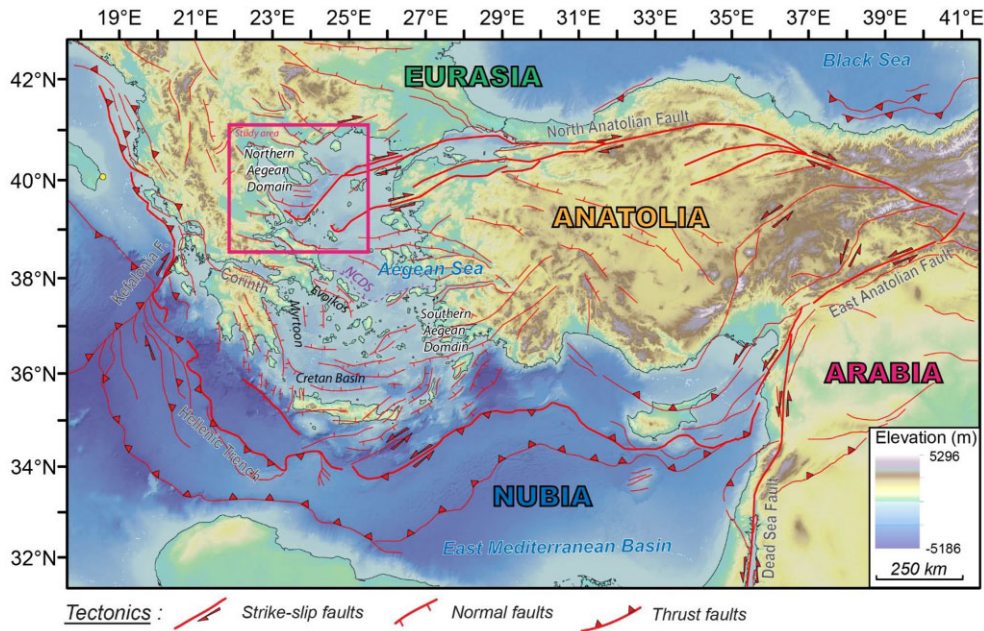


Figure 1. Tectonic framework of the Eastern Mediterranean Sea (active faults from Kreemer & Chamot-Rooke 2004 and Chamot-Rooke et al. 2005). The tectonic escape of Anatolia results from interactions between Arabia–Eurasia and the Hellenic trench retreat. NCDS, North Cycladic Detachment System.

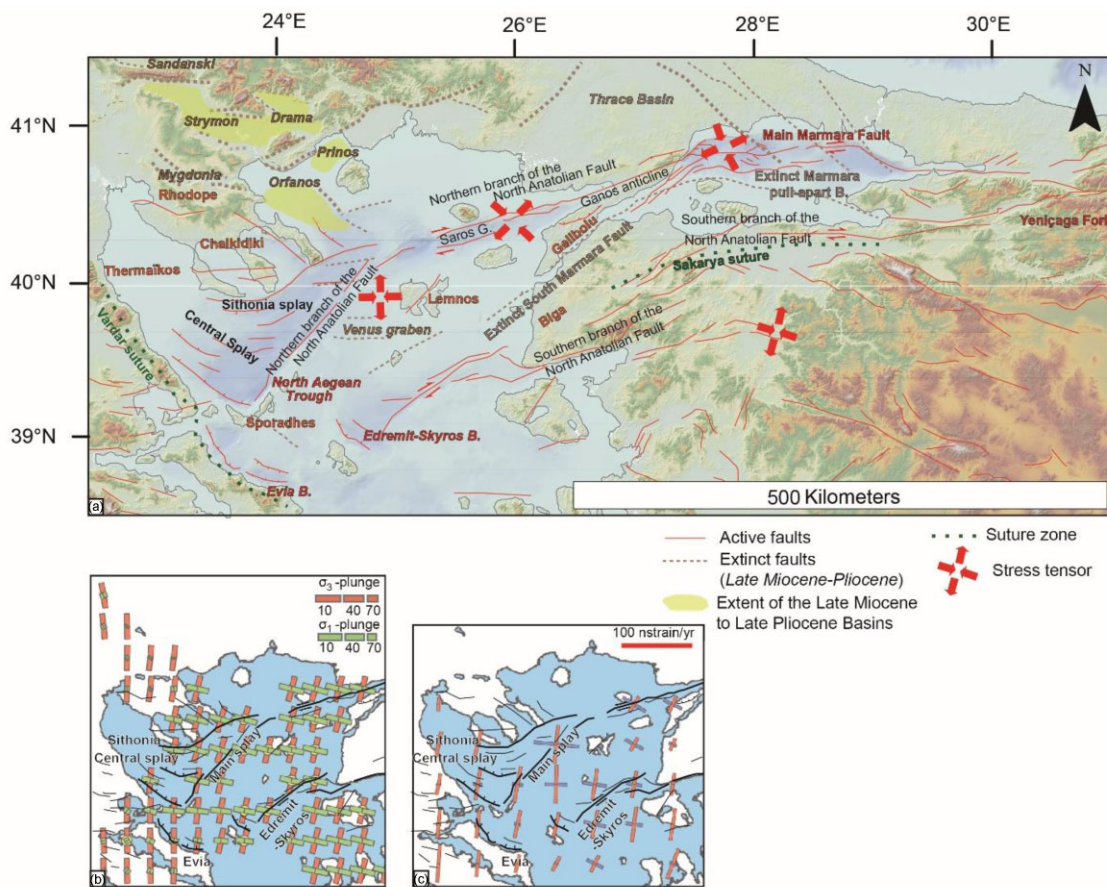


Figure 2. (a) Structural map of the segment of the North Anatolian Shear Zone in the North Aegean Domain, modified after Lyberis (1984), Koukouvelas & Aydin (2002), Yalçin et al. (2016); Sakellariou et al. (2018) and Papanikolaou et al. (2002; 2019). The stress tensors are from Gürer et al. (2016); Sümer et al. (2018). The location of the Late Miocene–Late Pliocene basins (Strymon, Mygdonia, Drama, Orfanos and Prinos) is from Brun & Sokoutis (2018). (b) Present-day stress tensors and (c) strain rate, from Floyd et al. (2010) and Konstantinou et al. (2017).

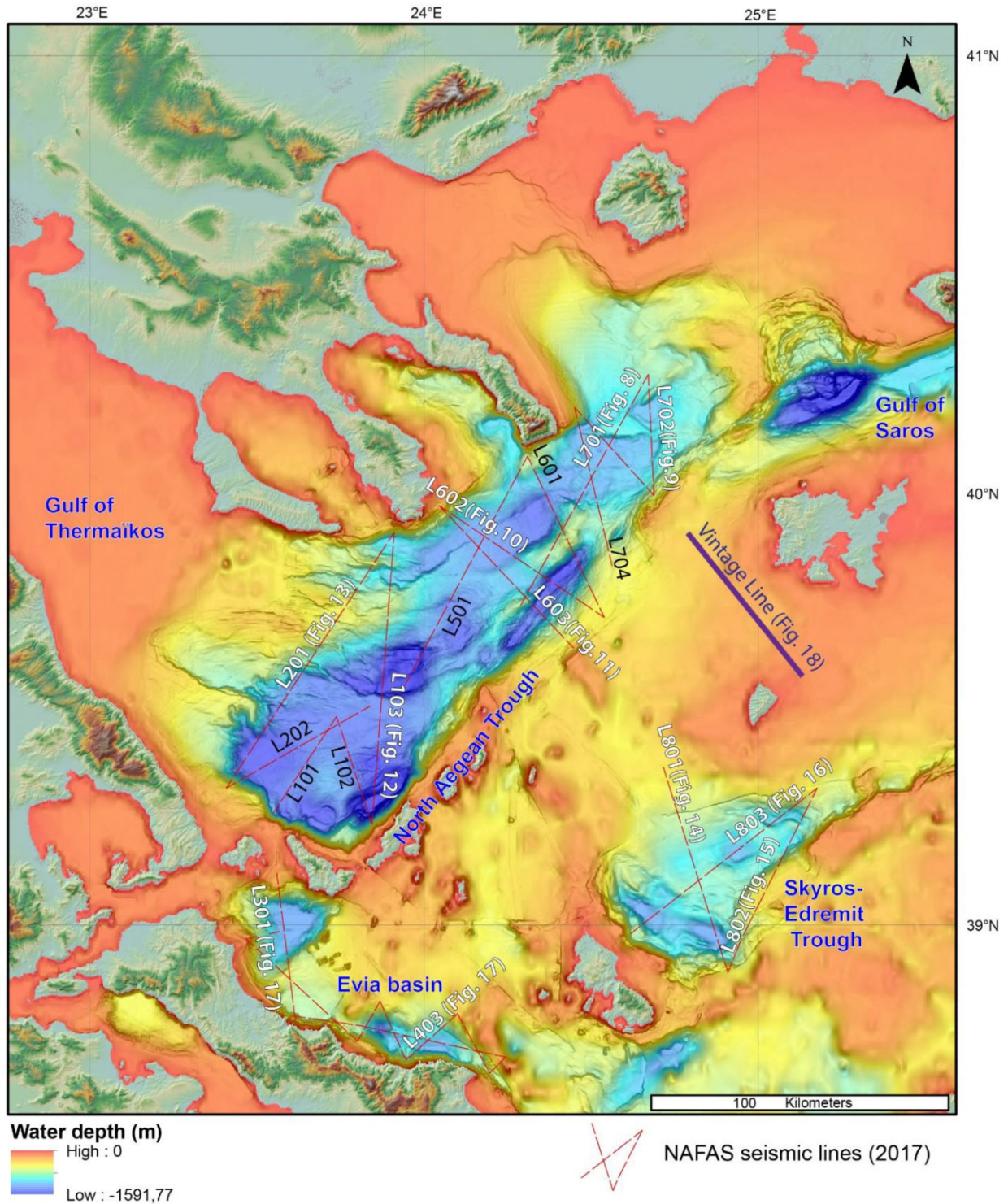


Figure 3. Topographic and bathymetric map of the North Aegean Domain and location of the seismic lines published in this study (Papanikolaou *et al.* 2002; Sakellariou *et al.* 2018, 2019).

On one hand, the North Aegean Trough is ~150-km-long, up to 80-km-wide and 1600-m-deep (Brooks & Ferentinos 1980; Papanikolaou *et al.* 2002; Ferentinos *et al.* 2018; Sakellariou *et al.* 2018), running from the Lemnos Deep to the Sporadhes archipelago (Figs 3 and 4). On the other hand, the Edremit-Skyros Trough is 70-km long,

up to 50-km wide and 1050-m deep (Figs 3 and 4; Papanikolaou *et al.* 2019). There, the southern branch of the North Anatolian Fault acts as a marginal structure, which bounds the southern flank of the trough over its entire length and splits into two 45- to 66-km-long oblique splays isolating sub-basins.

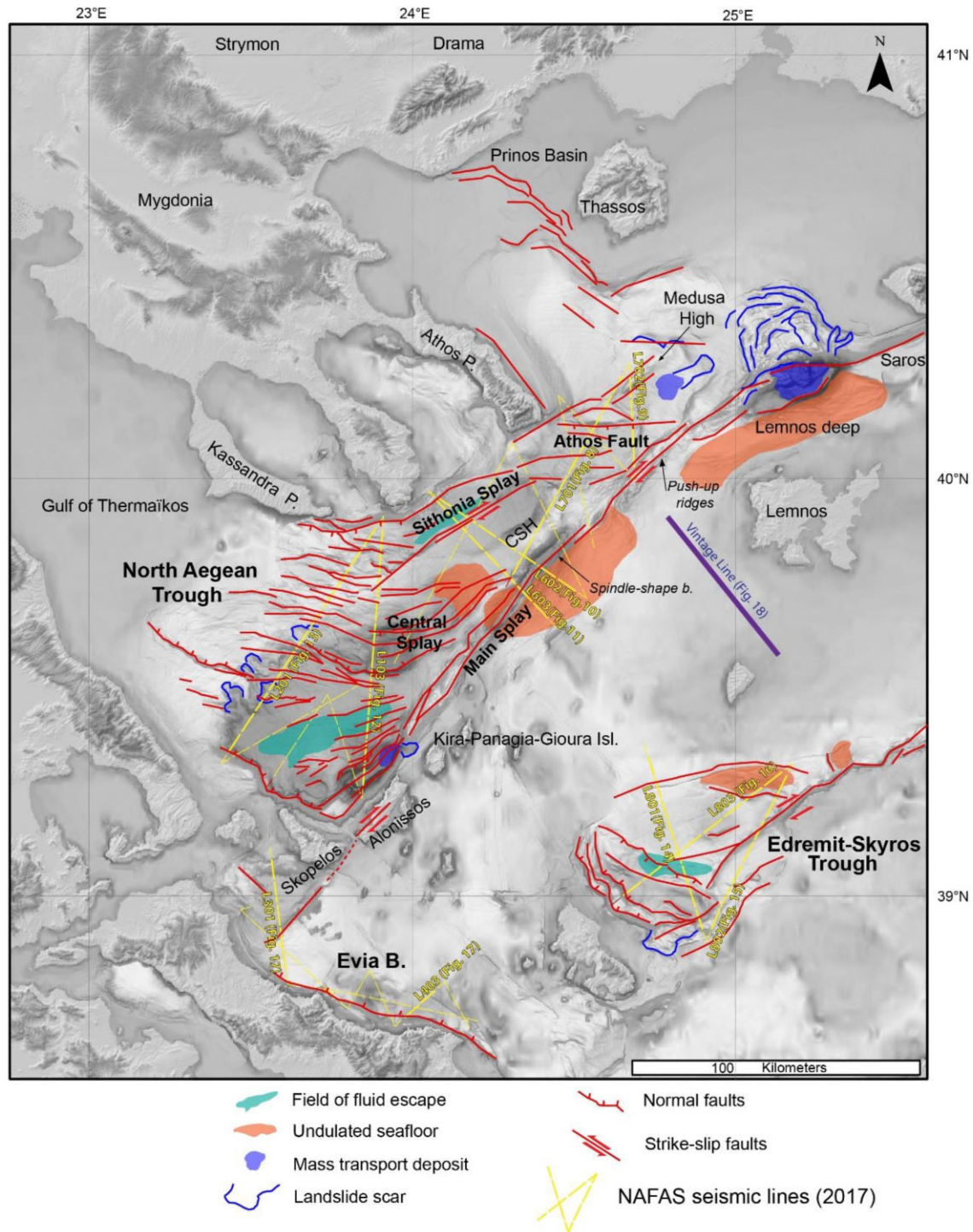


Figure 4. Structural map of the active faults of the North Aegean Trough and the Edremit-Skyros Trough and the main sedimentary features (modified after Papanikolaou *et al.* 2002; Sakellariou *et al.* 2018; 2019). CSH, Central Structural High.

2.2 Tectonic configuration of the North Anatolian Fault in the North Aegean domain since the Middle Miocene

The formation of the North Anatolian Fault results from the influence of several geodynamic drivers, including Arabia–Eurasia collision, the dynamics of the Hellenic trench retreat and the resulting differential in gravitational potential between the Anatolian plateau and the Aegean Sea (Jolivet & Faccenna 2000; Faccenna

et al. 2006; Brun & Faccenna 2008; Le Pourhiet *et al.* 2012; Jolivet *et al.* 2015; Brun *et al.* 2016; England *et al.* 2016).

Most of the constraints on the history of the North Anatolian Fault in the North Aegean Domain are based on the study of the Marmara Sea and its surroundings. At least three successive major strike-slip systems, evolving into a continuous frame of shearing of the continental lithosphere, have been identified on the basis of

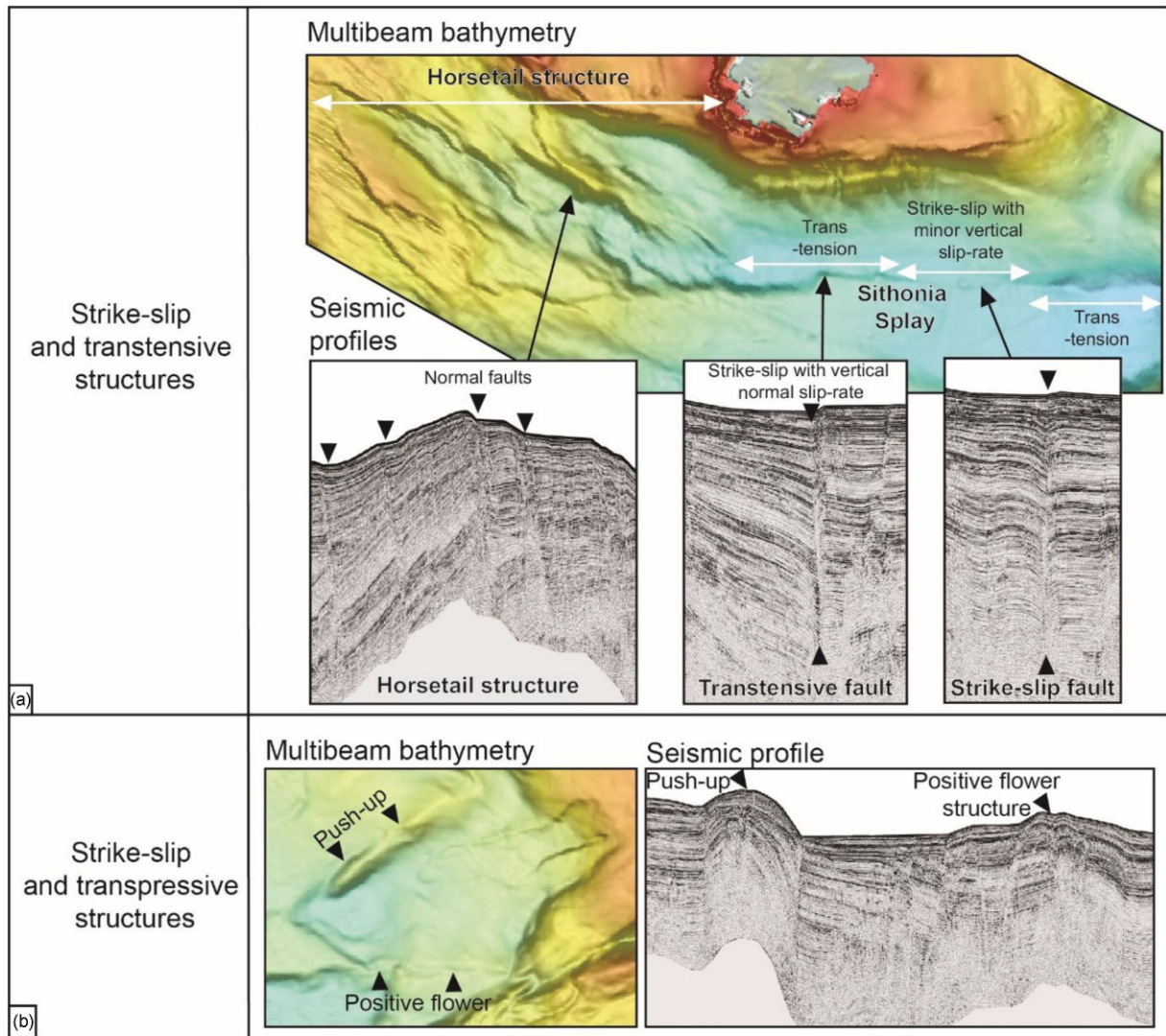


Figure 5. Criteria of identification of transpressive and transpressive strike-slip structures on the multibeam and seismic-reflection data set, with the examples of (a) the Sithonia Splay and (b) the Athos Splay.

seismic data tied to industrial wells (Le Pichon *et al.* 2014; Sengör *et al.* 2014, 2015).

A first diffuse strike-slip system emplaced in Late Serravalian–Tortonian (12–10 Ma), in the area that is now enclosed between the Thrace basin and the Sakarya suture (Fig 1 and 2). A part of this first strike-slip system is still active as the southern branch of the North Anatolian Fault, where the pattern of drainage networks recorded a structural reorganization around 0.5–1.3 Ma (Demoulin *et al.* 2013).

A second strike-slip system is evidenced at the South Marmara Fault and the Ganos segment, both corresponding to positive flower structures formed at a restraining bend (Fig. 2; Le Pichon *et al.* 2014, 2015; Karakas *et al.* 2018). These structures record the beginning of the localization of the North Anatolian Shear System in the Pliocene (Armijo *et al.* 1999; Le Pichon *et al.* 2014, 2015). The South Marmara Fault goes extinct around 3.5 Ma, while the Ganos segment is still active and forms a well-localized, >130-km-long dextral strike-slip fault (Armijo *et al.* 1999).

The third, localized strike-slip system corresponds to the northern branch of the North Anatolian Fault, expressed as the Main Marmara

Fault in the Marmara Sea (Le Pichon *et al.* 2001, 2003; Carton *et al.* 2007). Estimates of the age of the Main Marmara Fault range between 0.5 and 2.5 Ma (Rangin *et al.* 2004; Grall *et al.* 2012, 2013; Le Pichon *et al.* 2015). The Main Marmara Fault crosses the Gelibolu Peninsula and connects the Gulf of Saros at the entrance of the Aegean Sea through the Ganos strike-slip segment (Fig. 2; McNeill *et al.* 2004).

The age of formation of the North Aegean Trough and the Skyros–Edremit Trough is roughly constrained in the Late Pliocene–Early Pleistocene (Laigle *et al.* 2000; Beniès *et al.* 2016), a period which encompasses several stages of evolution of the North Anatolian Fault.

Onland, a series of sedimentary basins (Fig. 2; namely the Strymon, Orfanos, Prinos, Drama, Sandanski, Mygdonia basins and grabens) formed in the Serravalian segmenting the Rhodope Metamorphic Core Complex until the Early Pliocene (Brun & Sokoutis 2018). Traces of Late Miocene extension and differential subsidence are further observed in the Gulf of Thermaïkos and offshore the Chalkidiki peninsula (Varesis & Anastasakis 2021).

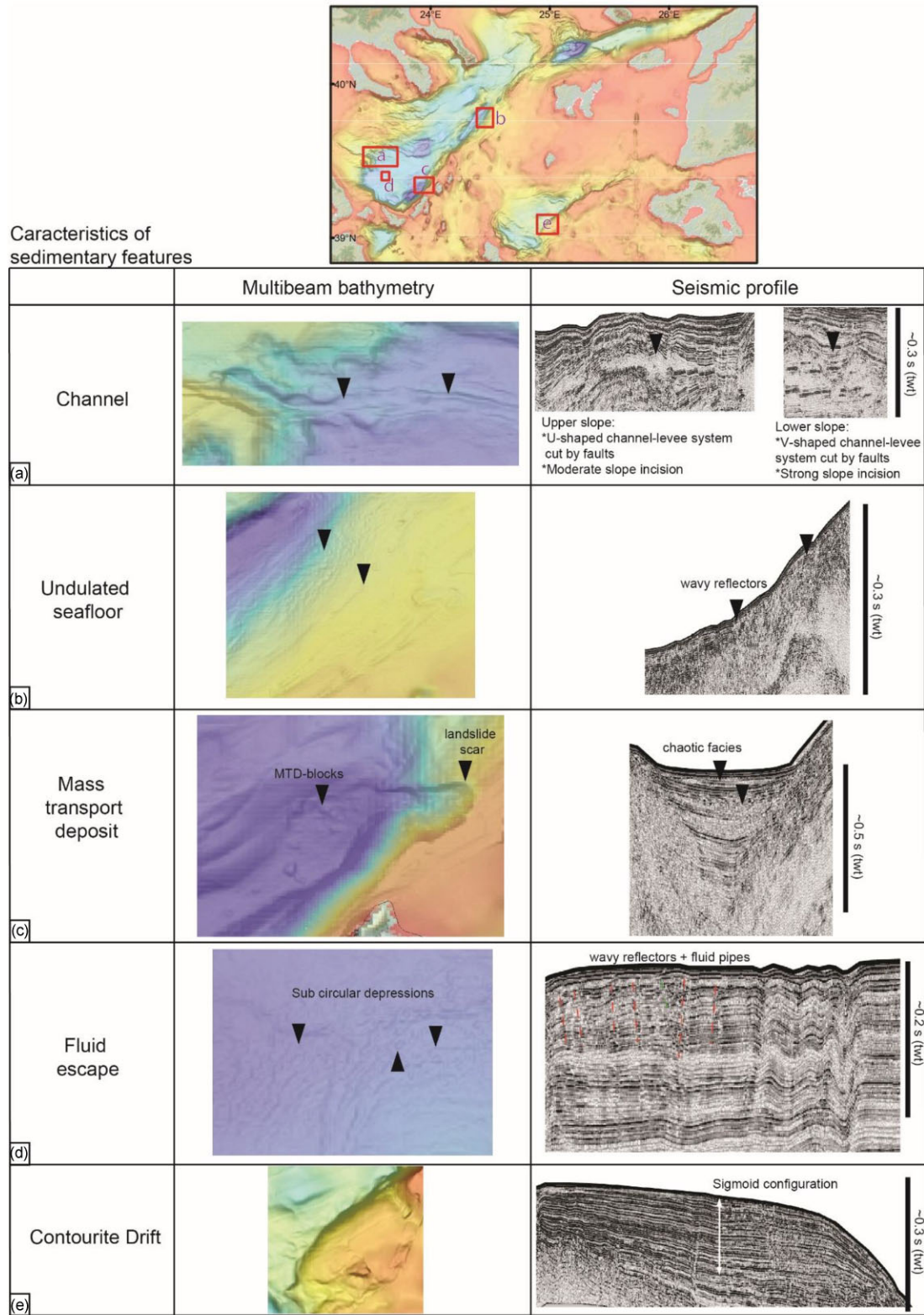


Figure 6. Classification of the facies of the main sedimentary features observed on the multibeam and seismic data set in the study area.

2.3 Structure of the lithosphere in the North Aegean domain

In the North Aegean Domain, the continental lithosphere keeps the record of a complex geological history, from the closure of

Mesozoic Oceans (i.e. the Vardar and Pindos Oceans, Schettino & Turco 2011; Okay & Tüysüz, 1999) to the building of the Hellenides Mountain Belt and its subsequent collapse in the wake of the Early Cenozoic collision between Adria and Pelagonia domains

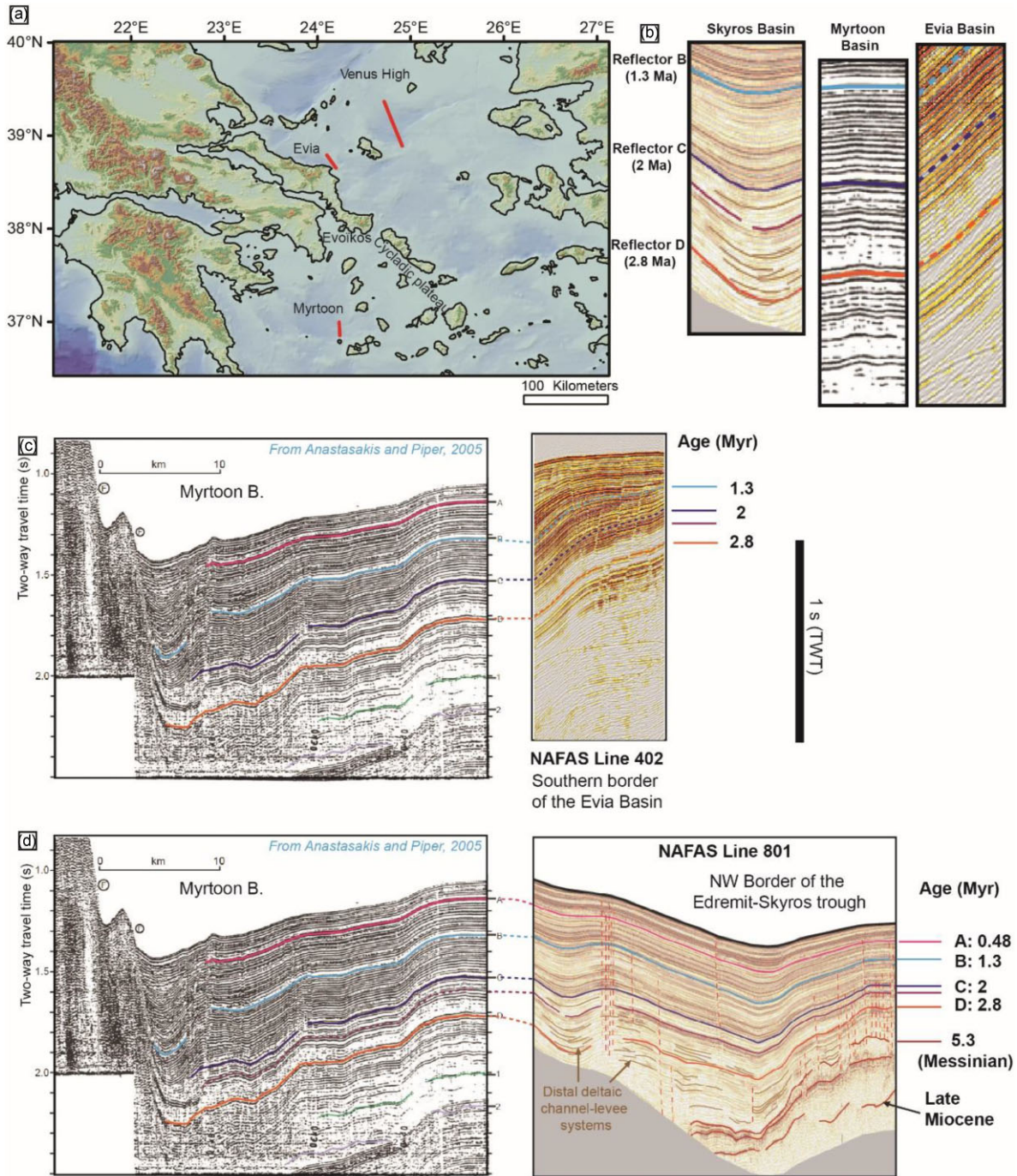


Figure 7. Stratigraphic correlation between the Myrtoon basin (Anastasakis & Piper 2005), the Evia Basin and the NW border of the Edremit-Skyros Trough.

(Handy *et al.* 2010). A series of metamorphic core complexes emplaced in the North Aegean Domain from the Late Eocene to the Middle Miocene (Rhodope Core complex, 45-Myr-old; North Cycladic Detachment System, 15–20-Myr-old; Jolivet & Brun 2010; Le Pourhiet *et al.* 2012; Jolivet *et al.* 2013).

As a result, the North Aegean lithosphere displays an unusual layering, with a shallow brittle ductile transition (<10 km,

Brun & Sokoutis 2018) and a thinned lithospheric mantle. The Moho depth ranges between 20 and 30 km (Sodoudi *et al.* 2006). Rayleigh wave anisotropy reveals the existence of a thermal anomaly located right in between the two segments of the North Anatolian Fault in the North Aegean domain, within the lower crust and the lithospheric mantle (Endrun *et al.* 2011).

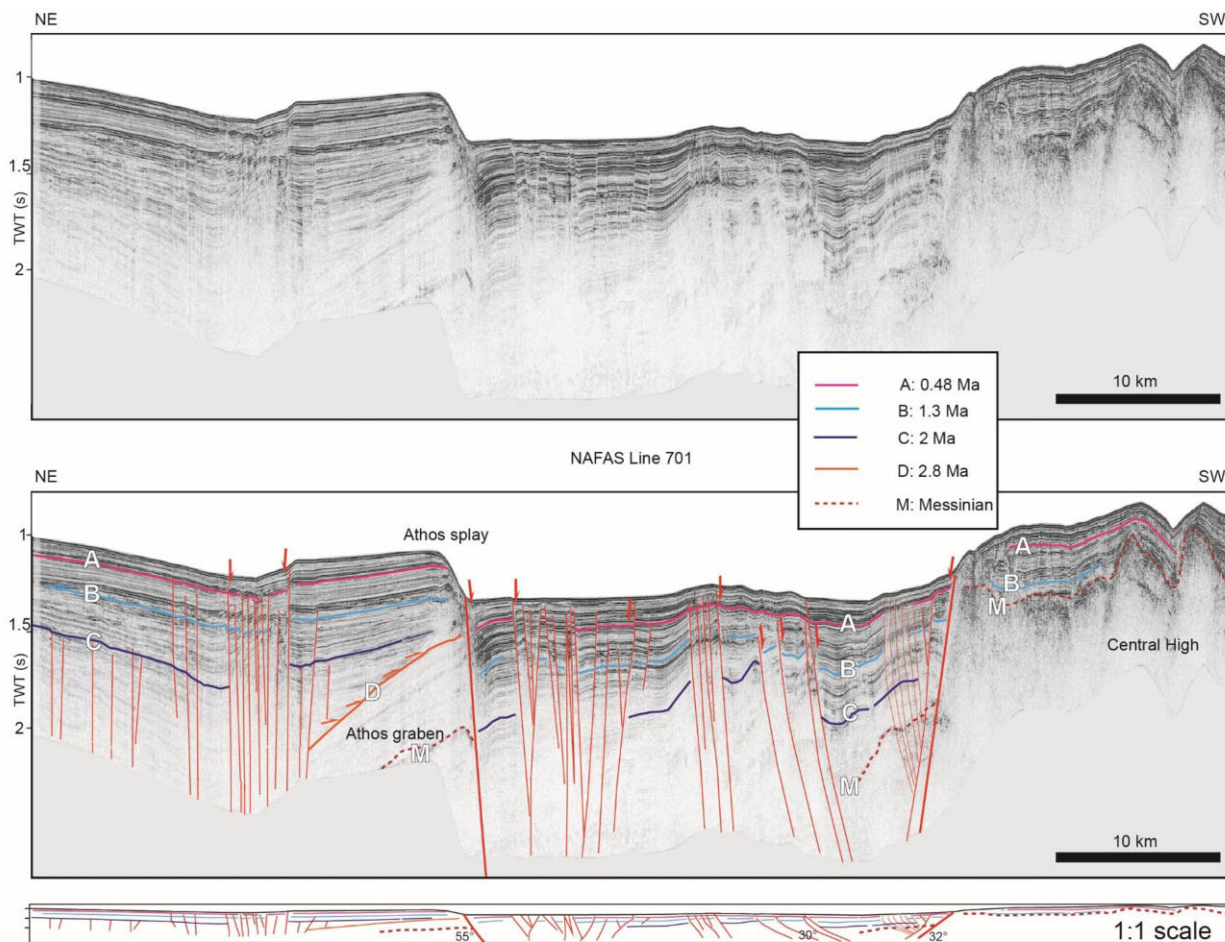


Figure 8. Seismic line 701 from the NAFAS cruise, crossing the Athos Splay and the North Anatolian Fault at the entrance of the North Aegean Trough. See Fig. 3 for location.

3 MATERIAL AND METHODS

3.1 Topography and seafloor bathymetry

The Digital Elevation Model used for the maps of the North Aegean Domain (Figs 1–4) combines data from the Shuttle Radar Topography Mission (SRTM) at 3 s and the multibeam data set acquired during the Ypothor oceanographic cruises between 2013–2016 (Sakellariou *et al.* 2018), here gridded at 25 m.

3.2 Seismic profiles

In this study, we present a new seismic-reflection data set collected during the NAFAS (North Anatolian Fault in the North Aegean Sea) expedition in summer 2017, onboard the R/V Tethys II. The expedition focused on the North Aegean Trough, the Edremit-Skyros Trough and the Evia Basin. The NAFAS data set is complementary documented by a set of vintage seismic-reflection data set collected in the 1970s and partly explored in Beniest *et al.* (2016). All the seismic-reflection profiles are displayed on the figures with a vertical exaggeration of 14, with their related simplified cross-section at 1:1 scale.

Seismic reflection profiles were shot using a GI airgun and a 24-trace streamer with 400-m maximum offset. The GI gun was triggered in harmonic mode (2×24 cubic inches) every 6 s, with an

acquisition speed of 4.1 knots, leading to a shot interval of 12.5 m. The trace record length is 5500 ms with a 1-ms sample interval. Only 8 out of 24 traces were working with a maximum offset of 200-m and a maximum CDP (Common Depth Point) fold of 4. The depth of penetration of the signal reaches about 3 s two-way travel time (TWT). The processing workflow consists in geometry setting, water-velocity normal moveout, stacking, deconvolution and Kirchhoff finite difference post-stack migration.

3.3 Multibeam and interpretation of geological structures on seismic-reflection profiles

The geological mapping of tectonic structures is based on the seafloor signature of the structure on the multibeam data and the expression of these features on the seismic-reflection lines (Fig. 5). The offshore structural maps provided in this study (Figs 4 and 5) are slightly modified from Papanikolaou *et al.* (2002, 2019) and Sakellariou *et al.* (2018), considering our new seismic data set.

The North Aegean Domain is dominated by a large variety of strike-slip structures (Fig. 5):

Negative flower structures: Most of the sub-basins isolated by the oblique splays within the horsetail terminations correspond to negative flower structures. The negative flower structures are bounded by normal faults of opposite dip and connect into a single strike-slip fault at depth.

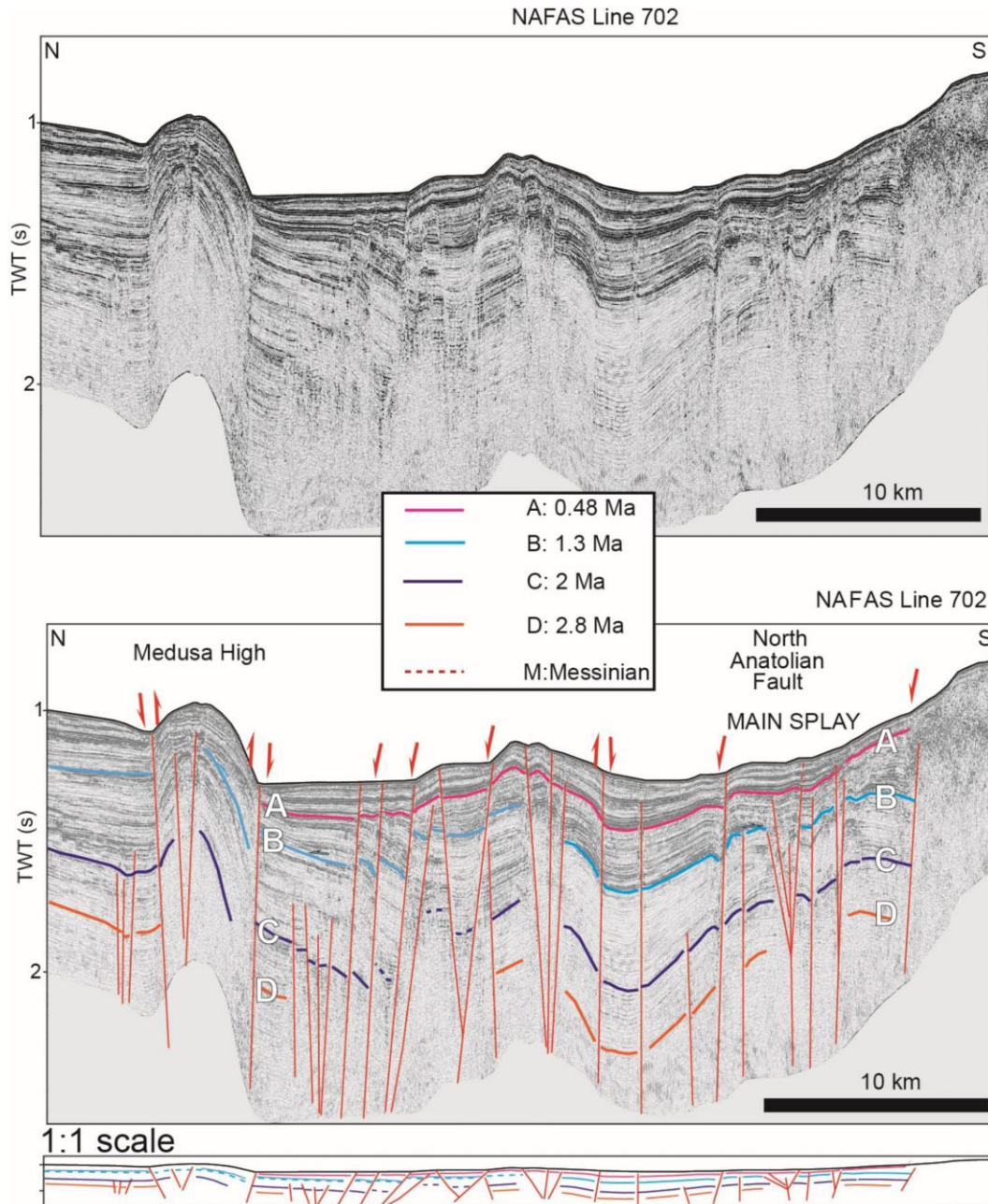


Figure 9. Seismic line 702 from the NAFAS cruise, crossing the Medusa High and the North Anatolian Fault. See Fig. 3 for location.

Transpressive structures: They correspond to positive flower structures and push-up structures, formed by a set of strike-slip faults with a reverse component.

Tectonic processes control the distribution of clastic sedimentary deposits in the study area (Fig. 6). Prior to the onset of the North Anatolian Fault, scattered distal deltaic rivers flood the area, marked by moderate incision along the thalweg. Since the onset of tectonic subsidence, the rivers form channel-levee systems close to the slope break and evolve downslope into canyons with V-shape morphologies (Fig. 6a). The complex distribution of faults and basins within the North Aegean Trough results in a scattered distribution of submarine landslides, identified according to their multibeam signature (arcuate scar and block falls at the edge of the slope, Fig. 6c) and their related mass transport deposits (marked a

chaotic-to-transparent seismic facies). Some of the steepest slopes display undulated seafloor (Fig. 6b), underlain by a series of wavy reflectors, which could be interpreted as sediment waves resulting from creeping of sediments in interaction with bottom-current controlled deposition (Faugères *et al.* 2002; Shillington *et al.* 2012). The tectonic structures also influence the circulation of oceanic bottom-currents. Where the current intensity is strong, the axis of the current is associated with a rough seafloor, which is an indicator of the strong sediment sorting. The attenuation of the intensity of the oceanic currents promotes the building of a series of fault-controlled contourite drifts (*sensu* Rebesco *et al.* 2014). The architecture of these contourite drifts display typical sigmoid to mounded configurations (Fig. 6e), characterized by important lateral thickness variations of the sedimentary layers, with pinched-out

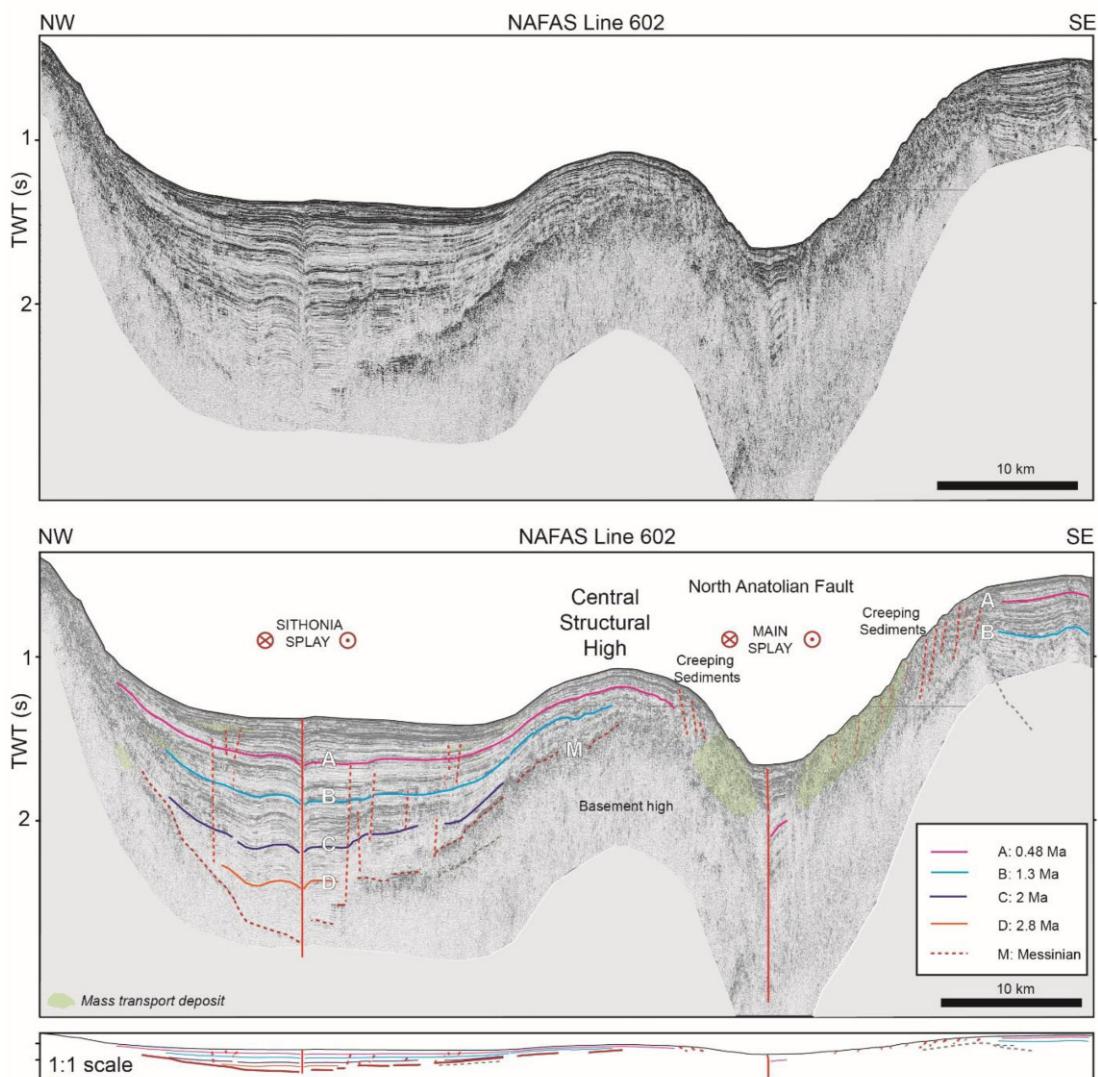


Figure 10. Seismic line 602 from the NAFAS cruise, crossing the main splay of the North Anatolian Fault, the central high and the Sithonia splay within the North Aegean Trough. See Fig. 3 for location.

reflectors close to the current axis and thicker deposits away from it. Fluid escape features are commonly observed close to the main faults and on the extrados of the main rollover structures (Fig. 4). Fluid escape features are expressed as dense networks of conduits leading to small offsets of the sedimentary layers or undulated to chaotic series of reflectors on the seismic data set (Fig. 6d). At the seafloor, the area of fluid escape form fields of coalescing circular depressions (Fig. 5e, Papatheodorou *et al.* 1993).

The clastic input to the North Aegean Sea implies that most of the structures related to the North Anatolian Fault are growth structures. The timing of formation of the strike-slip structures is constrained from the age of onset of the fanning of the sediments. Although many second-order unconformities linked to periodic sea-level and climatic variations are encountered in the study area (Lykousis 2009; Anastakis & Piper 2013), we here focus on the major unconformities corresponding to the main tectonic episodes related to the evolution of the North Anatolian Shear Zone, that is the unconformities corresponding to a significant tilt of the seafloor.

4 STRATIGRAPHY OF THE NORTH AEGEAN DOMAIN

4.1 The pre-Messinian period and the Messinian event

Field studies in the Thermaïkos, Thrace and Saros Basins document two Eocene to Oligocene silici-clastic units ontop of the metamorphic basement (Turgut & Eseller 2000; Siyako & Huvaz 2007; Islamoglu *et al.* 2008). Seismic profiles tied to wells evidence the continuity of these units offshore in the North Aegean Domain, with a major angular unconformity at the Oligocene-Miocene boundary (Beniest *et al.* 2016; Varesis & Anastakis 2021). Industrial wells located in the Prinos Basin (Proedrou & Papaconstantinou 2004) provide precise constraints on the ages of the geological events related to the Messinian Salinity Crisis, with the salt mobile unit dated between 5.97 and 5.33 Ma, and earliest traces of the Messinian stage dated around 7.15 Ma (Karakitsios *et al.* 2017).

We identify on the seismic data set the contact between the Late Miocene Unit and the Messinian Event according to the following criteria:

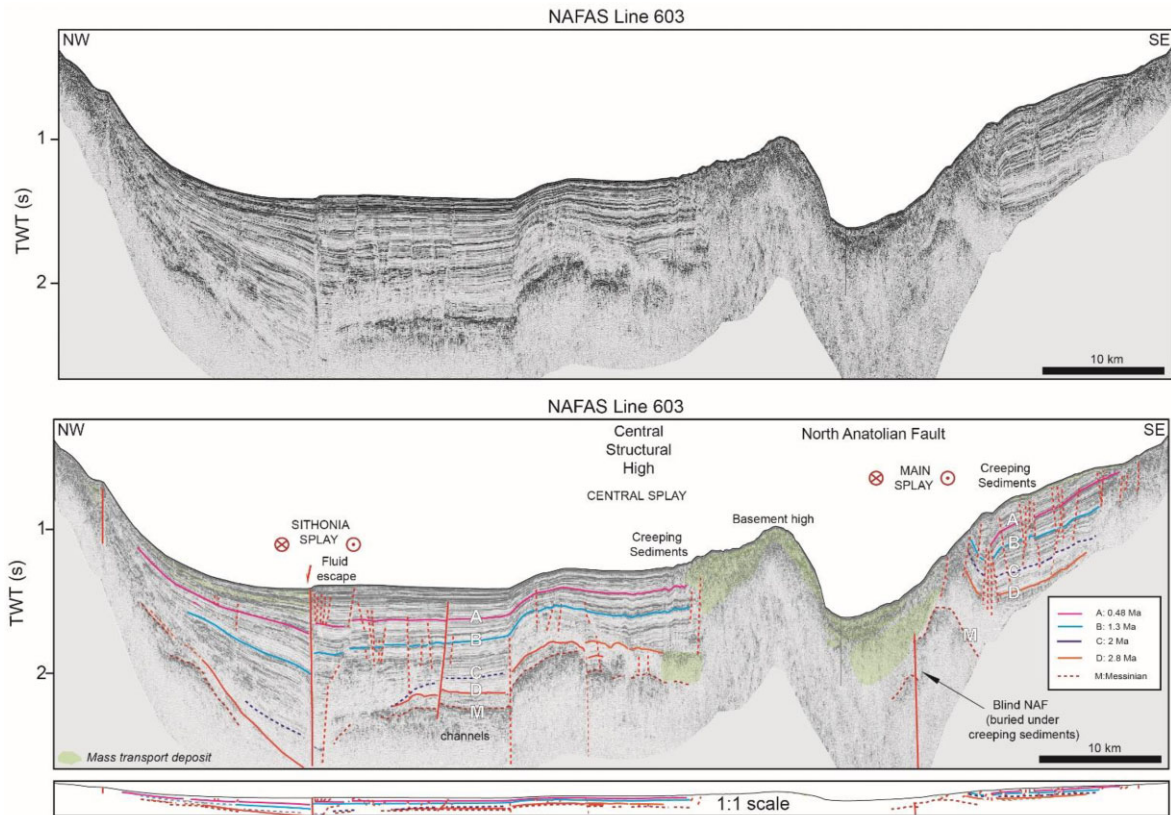


Figure 11. Seismic line 603 from the NAFAS cruise, crossing the main splay of the North Anatolian Fault, the central high and the Sithonia splay within the North Aegean Trough. See Fig. 3 for location.

Late Miocene Unit: During the Miocene, fluvial and floodplain deposits cover the North Aegean Domain (Melinte-Dobrinescu *et al.*, 2009; Suc *et al.* 2015). Drilling sites in the Prinos Basin that reach Tortonian layers document an alternation of marine shales and turbidites in a distal marine environment, followed by sandstone with marl and coal intercalations (Karakitsios *et al.* 2017; Varesis & Anastasakis 2021). On seismic data, the Late Miocene Unit is expressed by a series of interbedded channel systems (Fig. 7).

Messinian Event: The Messinian is dominantly expressed as an erosive surface in the North Aegean Domain (Fig. 7), with a few evaporitic units scattered in some basins (e.g. Prinos; Mascle & Martin 1990; Proedrou & Sidiropoulos 1992; Proedrou & Papaconstantinou 2004). Offshore Thermaïkos, the thickness of the Messinian Unit displays important lateral variations, culminating at 0.8 s TWT (Varesis & Anastasakis 2021).

4.2 Plio-pleistocene period

The Pleistocene stratigraphy has mainly been constrained on the basis of sequence stratigraphy studies, investigating the influence of sea level variations and oceanic current activity using the architecture of sedimentary bodies (Tripsanas *et al.* 2016; Sakellariou & Galanidou 2017). In the North Aegean Domain, sequence stratigraphy studies in the Thermaïkos Gulf (Lykousis 2009) and offshore the Biga Peninsula (Isler *et al.* 2008) identified the reflectors corresponding to MIS (Marine Isotopic Stage) 2 (18 ka) to MIS 12 (430 ka). Additional stratigraphic constraints are obtained from the study of contourite drifts in the Southern Aegean Domain since

MIS 11 (420 ka), with an increased current intensity, and hence, erosive events during interglacial periods (Tripsanas *et al.* 2016). In the vicinity of the North Aegean Trough, some coring document pro-delta formations during the Late Quaternary (last ~150 kyr; Piper & Perissoratis 1991; Lykousis *et al.* 2002).

Unfortunately, the published reports of the Prinos wells (Proedrou & Papaconstantinou 2004) do not provide stratigraphic details for the detritic Plio-Pleistocene sequence.

The only available stratigraphic constraints in the offshore Aegean Domain prior MIS12 are located at the Myrtoon Basin (Anastasakis & Piper 2005; Anastasakis *et al.* 2006), which is about 250-km away from our study area (Fig. 1). There, the age of the sedimentary layers is fairly well constrained as far as 2.8 Ma on the basis of correlation with DSDP Site 378 in the nearby Cretan Basin (Hsu *et al.* 1978) and the age of volcanic layers coming from Milos Island (Fytikas *et al.* 1976, 1986; Anastasakis & Piper 2005; Calvo *et al.* 2012). This set of reflectors is also observed offshore the Evoïkos Gulf (about 100–150 km away from our study area, Fig. 1) and their age is confirmed at 2 Ma upon the base of the sea level dependence of progradational packages of fluvial deposits (Anastasakis & Piper 2013). However, the Cycladic Plateau (Fig. 1, 7) has isolated the Myrtoon and Evoïkos area (Fig. 1) from the North Aegean Domain at various periods of sea level lowstands (Sakellariou & Galanidou 2017).

In order to investigate whether the stratigraphic constraints obtained at the Myrtoon Basin can be correlated as far north as the North Aegean Domain, we compare a seismic-reflection profile collected in the Myrtoon Basin (from Anastasakis & Piper 2005) with a profile collected at the southern termination of the Evia Basin,

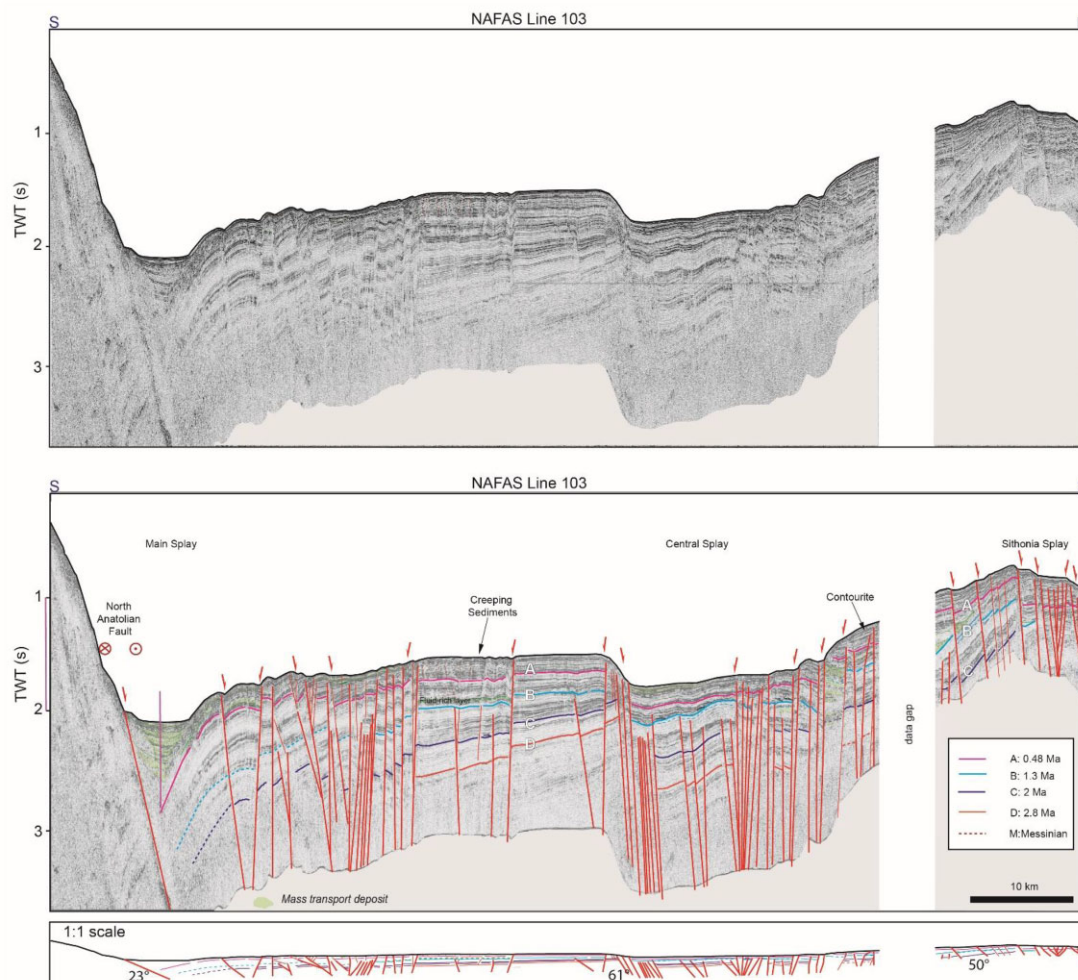


Figure 12. Seismic line 103 from the NAFAS cruise, crossing the Main splay of the North Anatolian Fault, the central splay and the western termination of the Sithonia Splay within the North Aegean Trough. See Fig. 3 for location.

that is north of the Cycladic Plateau, here considered as the key feature of the boundary between the north and south Aegean domains (Fig. 7). Despite a difference of resolution between the two data sets, both profiles share similarities with respect to the seismic facies of the Pliocene series up to a key reflector dated at 1.3 Ma (Fig. 7).

Based on sequence stratigraphy studies and correlation with the Myrtoon Basin, we consider that four Plio-Pleistocene key reflectors, corresponding to regional volcanic deposits and sapropel events (Anastasakis & Piper 2005), can be defined in the North Aegean Domain (Fig. 7), separating four main seismic units:

Reflector D (2.8 Ma): In the wake of the Messinian event, numerous Gilbert deltas developed in the surroundings of the Aegean Domain, followed by marine clastic sediments throughout the Pliocene, characterized by distal channel systems (Proedrou & Papaconstantinou 2004; Anastasakis & Piper 2005). Anastasakis & Piper 2005 show the regional transition from terrestrial to full marine facies occurred regionally at the boundary between the middle and upper Pliocene. A key reflector, labelled D, seals the seismic unit interpreted as the episode of delta fan supply in the Aegean Sea (Fig. 7; Anastasakis & Piper 2005). This seismic unit is character-

ized by the signature of distal channel-levee systems, marked by an alternation of minor downlap and onlap that reflects their successive avulsions. Reflector D is the top reflector of a series of three high-amplitude reflectors sealing the systems of delta fans. The reflector D is dated at ~2.8 Ma from Milos volcanics (Anastasakis & Piper 2005).

Reflector C (~2 Ma): Reflector C corresponds to an erosive surface, dated between 1.6 and 2.1 Ma from the volcanic deposits related to the Oros eruption (Pe-Piper *et al.* 1983; Dietrich *et al.* 1988). Sequence stratigraphy studies in the Evoikos Gulf suggest the age of reflector C to be closer to 2 Ma than 1.6 Ma (a reflector distinct from C being dated at 1.6 Ma, Piper & Anastasakis 2013). **Reflector B (~1.3 Ma):** Reflector B marks the onset of progradational wedges in the Aegean Sea, dated around 1–1.4 Ma with lava flows (Anastasakis & Piper 2005). The age has been refined at 1.3–1.4 Ma from sequence stratigraphy studies in the Evoikos Gulf (Anastasakis & Piper 2013).

Reflector A (~430–480 ka): Reflector A is defined by a set of sequence stratigraphic constraints available in the North Aegean Domain. It corresponds to MIS 12 (~430–480 ka). Our picking and spatial correlation of reflector A in the North Aegean Trough agrees with the work of Ferentinos *et al.* (2018).

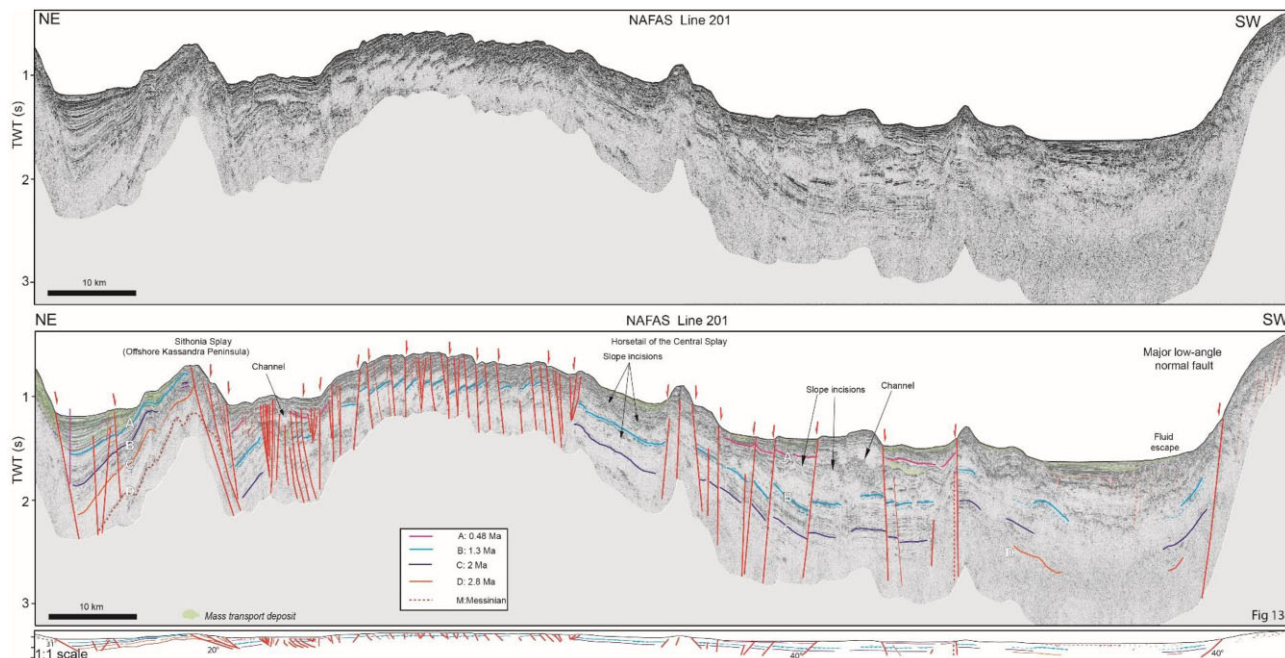


Figure 13. Seismic line 201 from the NAFAS cruise, crossing the series of oblique splays dissecting the slope at the edge of the Gulf of Thermaïkos and a field of fluid escape features. See Fig. 3 for location.

5 RESULTS

5.1 Structure of the North Aegean Trough (northern branch of the North Anatolian Fault)

5.1.1 The connection between the Gulf of Saros and the North Aegean Trough

At the northeastern entrance of the North Aegean Trough, the Main Splay of the North Anatolian fault makes a bend, which is expressed on the seafloor by a series of push-up ridges (Figs 3 and 4). The Main Splay forms a steep, $\sim 5\text{--}10^\circ$ slope, which is covered by an undulated seafloor. There, a set of secondary fault splays connects along the main fault. A 15-km-long ridge, referred to as the Medusa High (Masclé & Martin 1990; Sakellariou *et al.* 2018), runs parallel to the North Anatolian Fault in the area of bending (Figs 3 and 4). A second splay, referred to as the Athos Splay, runs at 40° with respect to the North Anatolian Fault and terminates at the tip of the Athos Peninsula (Figs 3 and 4).

Seismic line 701 is perpendicular to the Athos splay (Fig. 8) and seismic line 702 crosses the area between the main splay and the Medusa High (Fig. 9). The Main Splay runs across an area of chaotic reflectors and forms a flower structure. The Athos Splay is an apparent normal fault dipping at 55° southward, consistent with focal mechanisms at this location (Kiritzi & Louvari 2003). The footwall reveals a buried tilted block (Fig. 8). A dense network of normal faults, most of them being blind on the seafloor, connects into a set of three flower structures in the basin, located at the footwall of the Athos Splay (Fig. 8). The Medusa High (Fig. 9) corresponds to an elongated push-up structure (Masclé & Martin 1990; Sakellariou *et al.* 2018).

5.1.2 The central segment of the North Aegean Trough offshore the Chalkidiki Peninsula

The Main Splay of the North Anatolian Fault runs within a 40-km-long, 15-km-wide, asymmetric spindle-shaped trough (Fig. 3-4). Focal mechanisms confirm the strike-slip motion along the strike of the Main Splay and suggest a minor component of transtension locally (Kiritzi & Louvari 2003; Kourouklas *et al.* 2022). The Main Splay is subvertical and blind on the seafloor due to mass-wasting sedimentation rates higher than its vertical slip-rate (~ 0.4 -s TWT-thick package of mass transport deposits on Line 603; Fig. 11). It forms a growth-synform structure on Line 602 (Fig. 10) and promotes the uplift of the basement on line 603 (Fig. 11). The sedimentary cover of both flanks of the spindle-shape basin displays an undulated configuration upslope, which becomes more chaotic downslope.

The Sithonia Splay is a second strike-slip fault trending 60° NE. To the west, a network of normal faults, dipping 20° to the North, roots diagonally to the Sithonia Splay and forms a horsetail structure offshore the Kassandra Peninsula, where focal mechanisms indicate normal faulting (Kourouklas *et al.* 2022). The multibeam map reveals two sedimentary basins along the Sithonia Splay: a first one, located on the southern flank of the eastern segment of the fault and a second one, located on the northern flank of the western segment of the fault (Fig. 5). The Sithonia Splay is subvertical in its central part, forming a short-wavelength, symmetric growth-synform structure on Line 602 (Fig. 10). Line 603 indicates a strong component of subsidence with a well-marked fanning of the sediments on the northern side of the Sithonia Splay (Fig. 11). The westward increase of the subsidence corresponds to the transition towards the transtensional regime of the horsetail termination (Fig. 5).

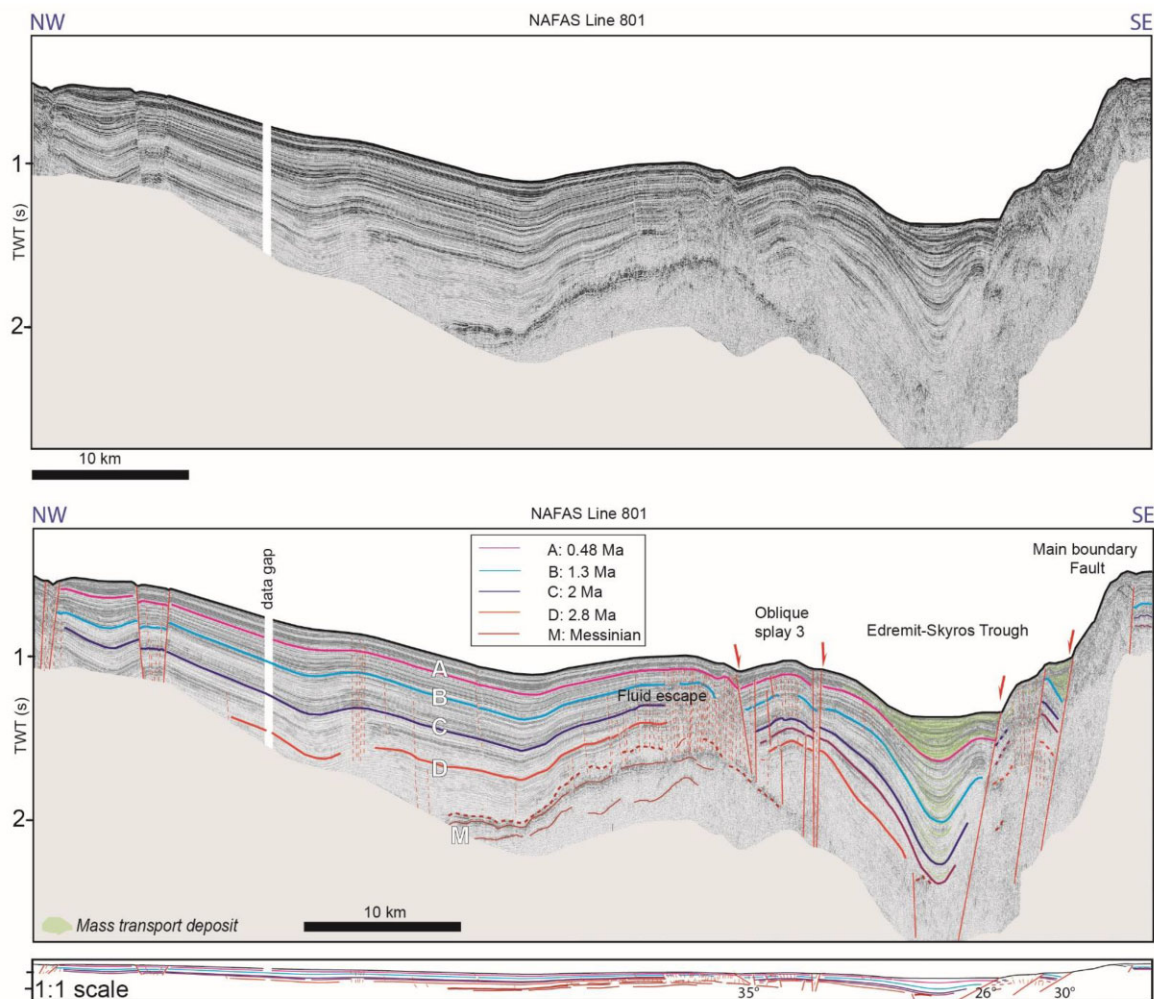


Figure 14. Seismic line 801 from the NAFAS cruise, crossing the Edremit-Skyros Trough. See Fig. 3 for location.

The Main Splay of the North Anatolian Fault and the Sithonia Splay are separated by a Central Structural High (Fig. 3-4). The Central Structural High is a ~50-km-long elongated feature, with two highs culminating at 700-m and 550-m depth. The Central Structural High appears as an antiform structure, with undulations in the sedimentary cover (Fig. 10-11). The part of the antiform which is still exposed at the seafloor corresponds to a basement high. A field of apparent normal faults with short and uneven offsets is observed between the Central Structural High and the Sithonia Splay (Figs 10 and 11).

5.1.3 Termination of the horsetail in the Thermaïkos-Skopelos area

Offshore Skopelos, the geometry of the Main Splay of the North Anatolian Fault changes from a strike-slip fault to a low-angle normal fault (Figs 3 and 4), which runs along Pelion and the Thermaïkos Gulf (Laigle et al. 2000). The seismic reflection profile 103 (Fig. 12) crosses all the splays from Skopelos Island to Kassandra Peninsula. We observe a large-scale rollover structure in the hanging wall of the North Anatolian Fault, bending along the Main Splay, acting here as a north-dipping low-angle (~20°) normal fault. Focal mechanisms however indicate pure strike-slip motion in this area (Kourouklas et al. 2022), which suggests that the normal fault is turning into

a strike-slip fault. The configuration of the low-angle normal fault isolates a 20-km-long, 10-km-wide trough along the Main Splay, filled-in by mass transport deposits (Fig. 12). The hinge of the rollover is dissected by numerous synthetic and antithetic normal faults. These fault systems cross a field of coalescing circular depressions spreading over ~200 km², which corresponds to a series of short-wavelength undulated reflectors on the seismic, focused on the uppermost ~0.4 s TWT (Fig. 12). The field of circular depressions is interpreted as the result of fluid escape (Figs 3 and 4).

The Central Splay (Figs 3 and 4), roots on the Central Structural High, then bends across the extrados of the rollover into a 25-km-long, 15-km-wide, 1450-m-deep trough, formed by a system of normal faults. The normal fault scarps reach 350-m-high at the seafloor along the slope of the Gulf of Thermaïkos and localize a system of slope-apron canyons.

The seismic line 201 (Fig. 13) crosses the area between the major low-angle (~35° dip) normal fault where the North Anatolian Fault ends and the termination of the Sithonia Splay. The hanging wall forms a syncline basin, filled-in by sediments characterized by the short-wavelength undulated facies formed by fluid escape. The system of normal faults crossing the slope of the Gulf of Thermaïkos forms a series of horst and graben (Fig. 13). The termination of the Sithonia Splay is a set of two sub-parallel listric faults, dipping

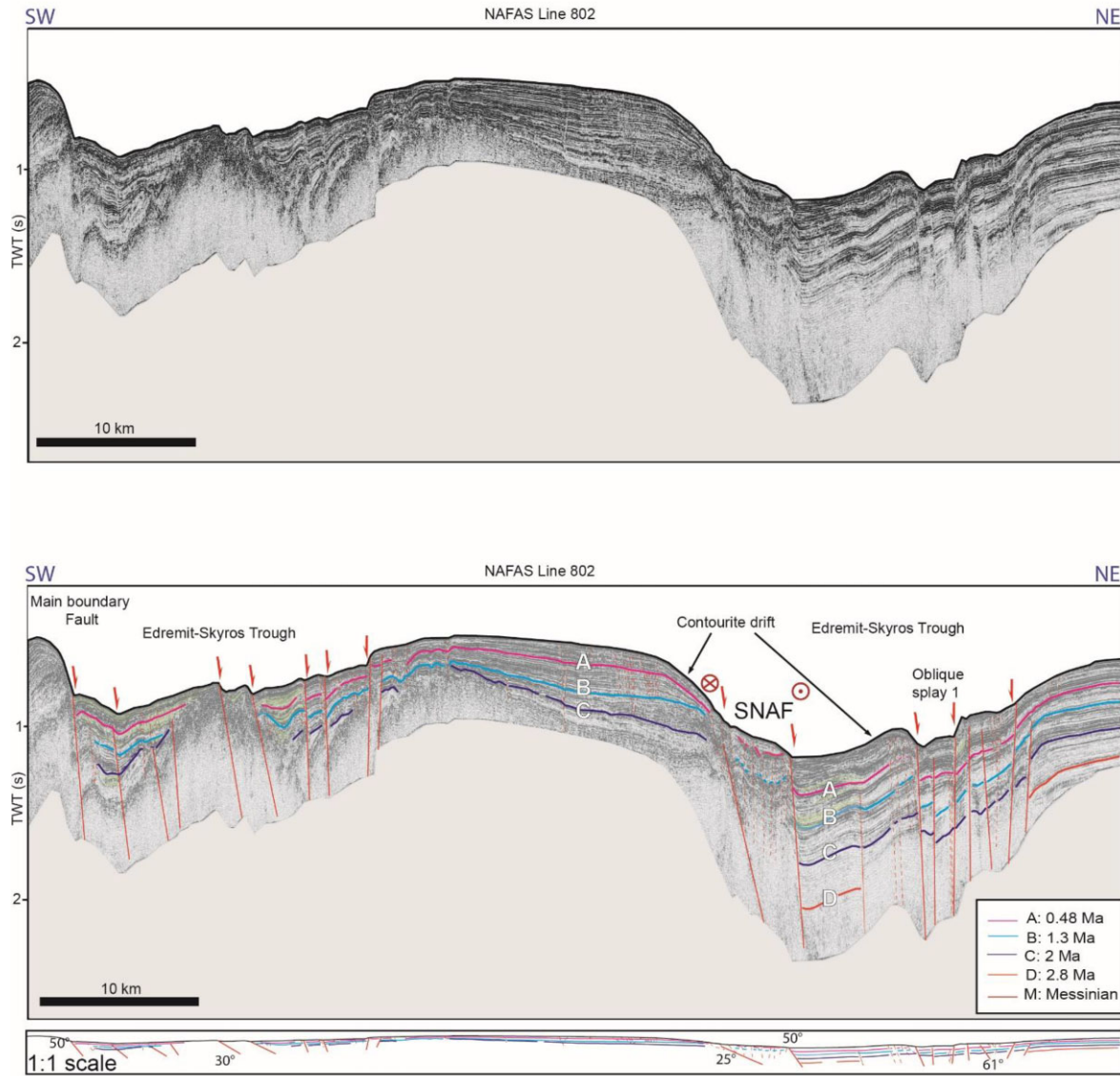


Figure 15. Seismic line 802 from the NAFAS cruise, crossing the Edremit-Skyros Trough. See Fig. 3 for location.

20° to 30° to the north, with their associated rollover structures dissected by synthetic and antithetic normal faults (Fig. 13), consistent with the focal mechanisms at this location (Kourouklas *et al.* 2022).

5.2 Structure of the Edremit-Skyros Trough (southern branch of the North Anatolian Fault)

The structure of the Edremit-Skyros horsetail is described in details in Papanikoalou *et al.* (2019). In this study, we present three new seismic profiles, which cross all the key structures of the Edremit-Skyros Trough.

The seismic profile 801 (Fig. 14) crosses the Venus plateau, an oblique splay of the horsetail, the deepest basin of the trough, here expressed as a growth syncline, and the main system of subparallel low-angle (~25° dip) normal faults bounding the Skyros Island, which isolates a half-graben. The seismic line 802 (Fig. 15) crosses the southern branch of the North Anatolian Fault and the southern edge of the Edremit-Skyros Trough. It reveals a series of angular

unconformities associated to tilted blocks. On the seismic profile 803 (Fig. 16), the oblique splays of the horsetail appear as normal faults isolating either half-grabens or growth synclines, dominantly filled-in by mass transport deposits. The subsidence increases towards the Skyros Island. Normal faults segment the bulge of the growth-synclines. In this area, sedimentation rates exceed the vertical slip-rate at the faults, resulting in their smooth aspect on the seafloor.

5.3 Structure of the Evia basin

The Evia basin consists in a 90-km-long series of three subsiding basins, up to 1000-m deep, separated by structural highs (Fig 3-4). On the seismic lines (Fig. 17), all the Evia sub-basins appear as a series of tilted half grabens bounded by a major normal fault on their SW flank. The maximum thickness of the post-Messinian sediments reaches ~1 s (TWT). The series emplaced before the formation of the structure display seismic facies typical of distal detritic sedimentation, while the syn-tectonic series display a

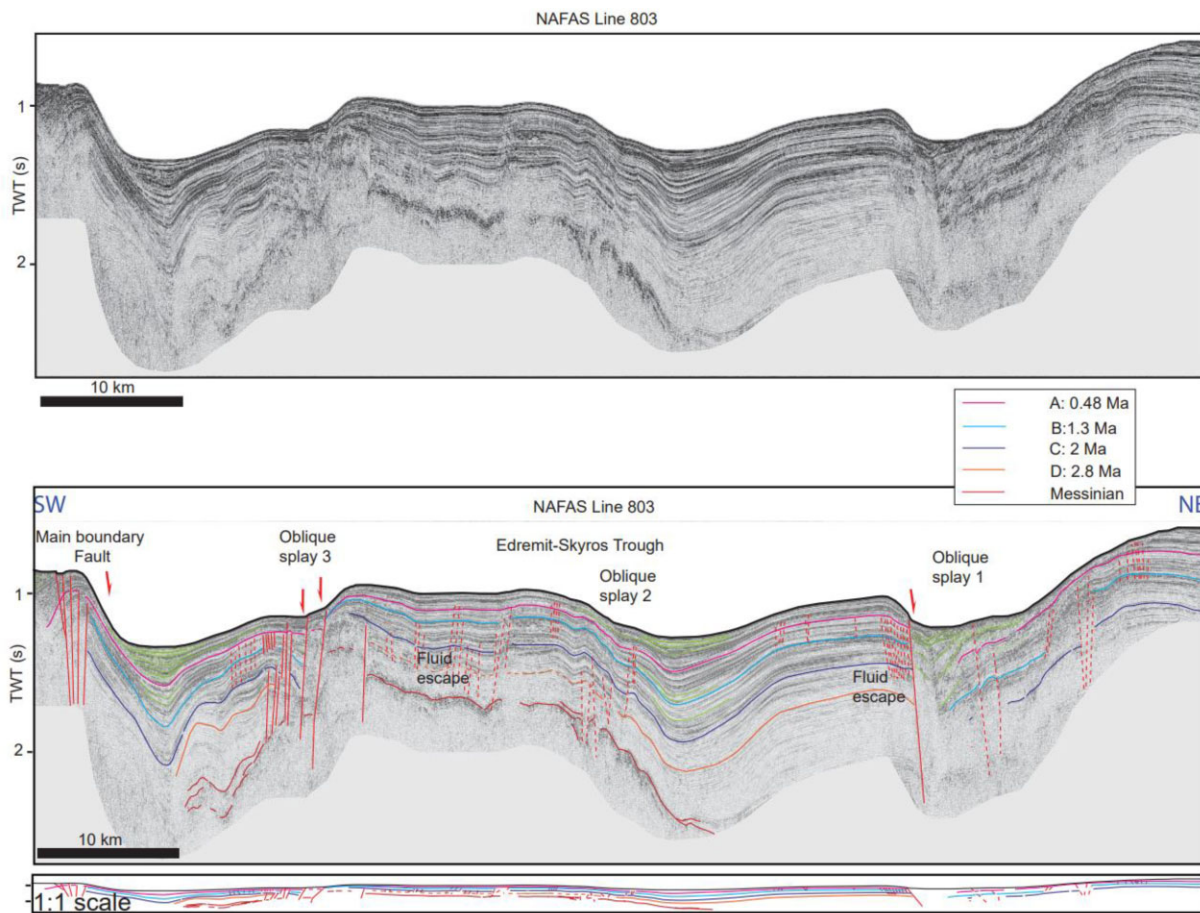


Figure 16. Seismic line 803 from the NAFAS cruise, crossing the Edremit-Skyros Trough. See Fig. 3 for location.

fanning configuration recording the progressive subsidence of the structure. Only minor Mass Transport Deposits are observed within the growth structures, which results from the $\sim 20^\circ$ steep slope formed by the main normal fault that does not allow the storage of sediments. The structural thresholds appear as positive flower structures in line with the trend of the North Anatolian Fault, with uplifted segments of the basement and a dense pattern of faults on their flanks.

5.4 A diffuse fault system buried in the offshore North Aegean domain

The seismic lines collected during the NAFAS cruise in 2017 together with the compilation of vintage seismic lines (Masclé & Martin 1990; Beniést *et al.* 2016) reveal fossil structures buried under the sediments of the North Aegean Domain and locally crosscut by the horsetail structures.

The first structure is encountered in the area of the connection between the Saros Gulf and the North Aegean Trough, at the W–E trending Athos splay (Figs 3 and 4). There, the seismic line 701 (Fig. 8) reveals a buried tilted block sealed by a series of onlap terminations of the sedimentary layers.

The second structure also corresponds to a tilted graben, located at the plateau isolated between the North Aegean Trough and the Edremit-Skyros Trough (Fig. 18). This graben is referred to as the Venus graben.

5.5 Chronology of tectonic events in the North Aegean Sea

The series of angular unconformities labelled from A to D records the main tectonic events that shaped the North Aegean Domain since the Messinian (Fig. 7).

5.5.1 The North Aegean Trough

Unconformity D, dated at 2.8 Ma, records the end of the tectonic episode expressed by the series of tilted blocks composed of the Athos (Fig. 8) and Venus (Fig. 18) grabens. This unconformity also marks the deactivation of a series of push-up structures located in the area of the Central Structural High (line 603, Fig. 11). At the termination of the Sithonia Splay (line 201, Fig. 13) offshore Kassandra Peninsula, this unconformity marks the onset of a fanning configuration of the sediments and, therefore, the onset of the tilt of the graben.

The second key angular unconformity C, dated at 2 Ma, is well identified by onlap terminations over the underlying, tilted deposits in the North Aegean Trough (e.g. in the vicinity of Skopelos at line 103, Fig. 12). This unconformity marks the onset of the fanning configuration of the sediments observed all along the Sithonia Splay (line 201, Fig. 13; line 602–603, Figs 10 and 11), and hence, the formation of this still-active splay within the North Aegean Trough. The amplitude of slope incision features remains poorly disturbed by this tectonic episode (e.g. at the edge of the Thermaïkos Gulf, line 201, Fig. 13), which indicates a still rather low subsidence rate.

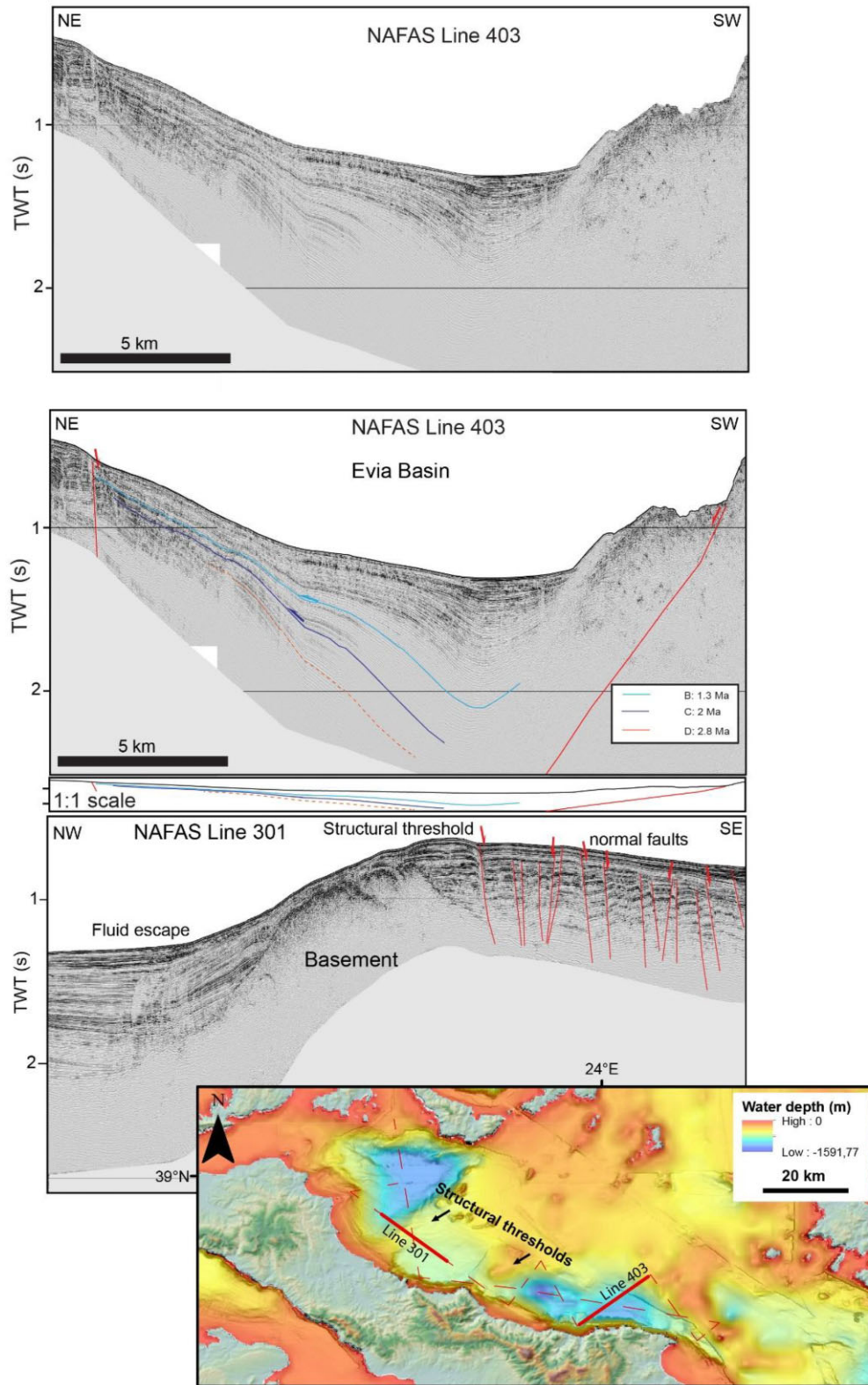


Figure 17. Seismic line 401 from the NAFAS cruise, crossing the main normal fault bounding the Evia Basin and seismic line 301 crossing one of the structural thresholds identified within the Evia basin. See inset and Fig. 3 for location.

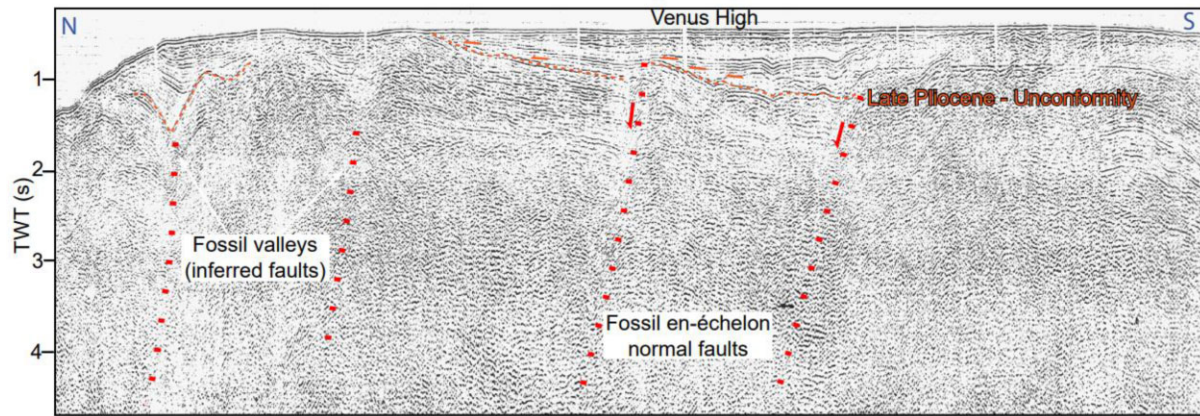


Figure 18. Vintage seismic line, from Beniést *et al.* (2016), showing the Venus graben. See Fig. 3 for location.

These unconformities D and C record the Late Pliocene–Early Pleistocene change in the pattern of strain localization within the North Anatolian Shear Zone. These unconformities also pre-date the first stage of the formation of the North Aegean horsetail structure, with the activation of the Sithonia Splay.

The third angular unconformity B, dated at ~ 1.3 Ma, records the formation of the termination of the central splay (observed at line 103, Fig. 12). Across the edge of the Thermaïkos Gulf, the 1.3-Myr-old unconformity corresponds to an increase in the amplitude of the slope incisions features (line 201, Fig. 13), which indicates a major increase in the overall subsidence, the channels digging deeper to catch their equilibrium line. The Mass Transport Deposits associated to this episode are the thickest (~ 0.2 – 0.3 s TWT) encountered within the North Aegean Domain since the Messinian. At the connection between the North Aegean Trough and the Saros Gulf, the 1.3-Myr-old unconformity records the formation of the Athos Splay and the main uplift of the Medusa High (Fig 8-9). There, the mean vertical slip-rate of the Athos normal fault increased from a 0.13 mm yr^{-1} during the 2–1.3 Ma interval to 0.22 mm yr^{-1} since 1.3 Ma. Overall, this set of observations indicates a major structural reorganization of the northern branch of the North Anatolian Fault at 1.3 Ma, marked by a drastic increase in subsidence rates within the sub-basins of the North Aegean Trough.

Finally, unconformity A, dated at ~ 0.5 Ma, records the onset of the Main Splay of the North Anatolian Fault all across the North Aegean Trough (Ferentinos *et al.* 2018). The formation of the Main Splay is best recorded offshore Skopelos (line 103, Fig. 12), the segment of the fault running at the edge of the Central High being affected by current and gravity-driven erosion (line 602, Fig. 10). The activation of the Main Splay induced a change in the activity of the Sithonia Fault, with an increase of the vertical slip-rate from 0.16 mm yr^{-1} during the 1.3–0.48 Ma interval to 0.3 mm yr^{-1} since 0.48 Ma. However, the vertical slip-rate of the faults related to the Central Splay remained steady.

5.5.2 The Skyros-Edremit Trough

The unconformity C (2 Ma) is onlapped by a tilted series of reflectors on the southern edge of the trough (line 803, Fig. 16). This unconformity marks the first stages of the formation of the Southern branch of the North Anatolian Fault offshore Skyros. Unconformity B (1.3 Ma) corresponds to the increase in the subsidence rate (up to 0.45 mm yr^{-1}) at the hanging wall of the normal fault system running along Skyros Island (Figs 14–16). Unconformity A (~ 0.5 Ma)

is well expressed close to the oblique splay 1 and marks an increase in subsidence at the hanging wall of this splay (Fig. 15). Unconformity A therefore records the formation of the oblique splay 1 (Fig. 16).

5.5.3 The Evia Basin

The onset of subsidence within the Evia Basin is dated between 2 and 1.3 Ma based on unconformities B and C (Fig. 17). This marks the base of the fanning configuration of the sedimentary infill. The main formation episode of the Evia Basins is therefore coeval with the increase in subsidence at Corinth and the first step of strain localization at both the northern and southern branches of the North Anatolian Fault.

6 DISCUSSION

The present-day configuration of the North Aegean Domain shows the gradual kinematic transition from the strike-slip deformation that dominates in the northeastern Aegean Domain to the dip-slip deformation encountered in the Northwest Aegean Domain (Mouslopoulou *et al.* 2007a,). Our new set of geological constraints allows us to refine the framework of strain localization of the North Anatolian Shear Zone in the North Aegean Domain and highlights the westward propagation of the strike-slip dominated area since the Late Miocene. The new geological constraints obtained from the seismic-reflection data set are summarized in Fig. 19 and integrated to the previously available constraints on the geological events of the area.

6.1 Mode of formation of horsetail structures: the North Aegean and Edremit-Skyros Troughs

The formation of the horsetail terminations of both the northern and southern branches of the North Anatolian Fault occurs in the frame of the westward propagation of the North Anatolian Fault within the prevailing NNE–SSW to N–S extensional conditions of the western North Aegean Domain. The horsetail configuration emplaces where the strike-slip fault connects a system of low-angle normal faults inherited from the extensive stage.

The North Aegean and the Edremit-Skyros Troughs are horsetail terminations that are currently at different steps of their development. Although the formation of both structures initiated at the same age (~ 2 Ma), the lower slip rate along the southern branch of the

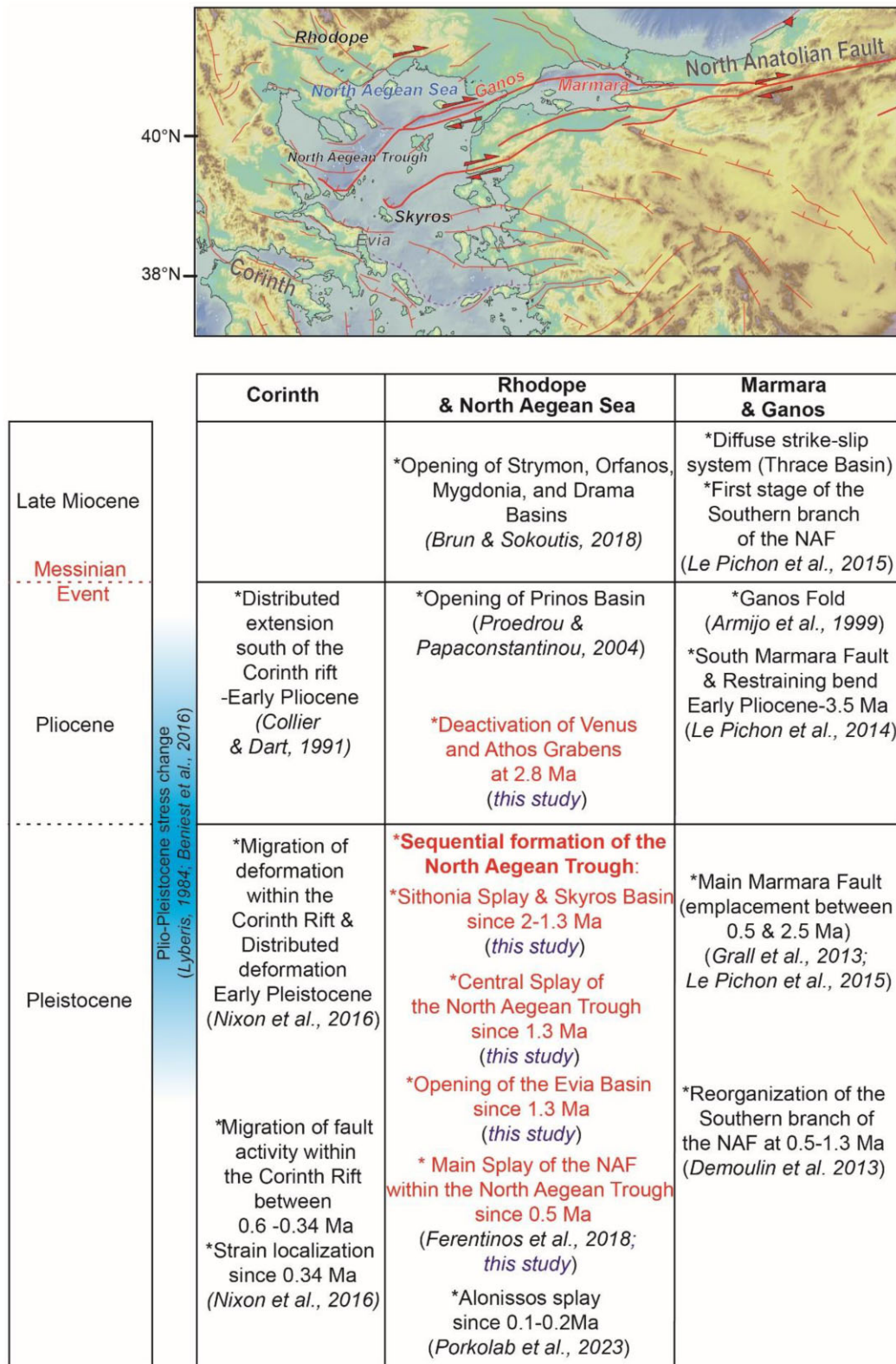


Figure 19. Summary of the main steps of structural evolution of the North Anatolian Fault and the Gulf of Corinth in the North Aegean Domain (Collier & Dart 1991), Ford et al. 2013, Nixon et al. 2016 and Porkoláb et al. 2023.

North Anatolian Fault leads the Edremit-Skyros to be structurally less mature. This differential stage of horsetail structural evolution allows us to investigate the tectonic and sedimentary processes at their origin.

On one hand, the Edremit-Skyros Trough corresponds to the evolution of a single horsetail structure. The oblique splays of the Edremit-Skyros Trough formed first along the main detachment fault, then migrated eastwards (oblique splay 1 formed at 0.5 Ma).

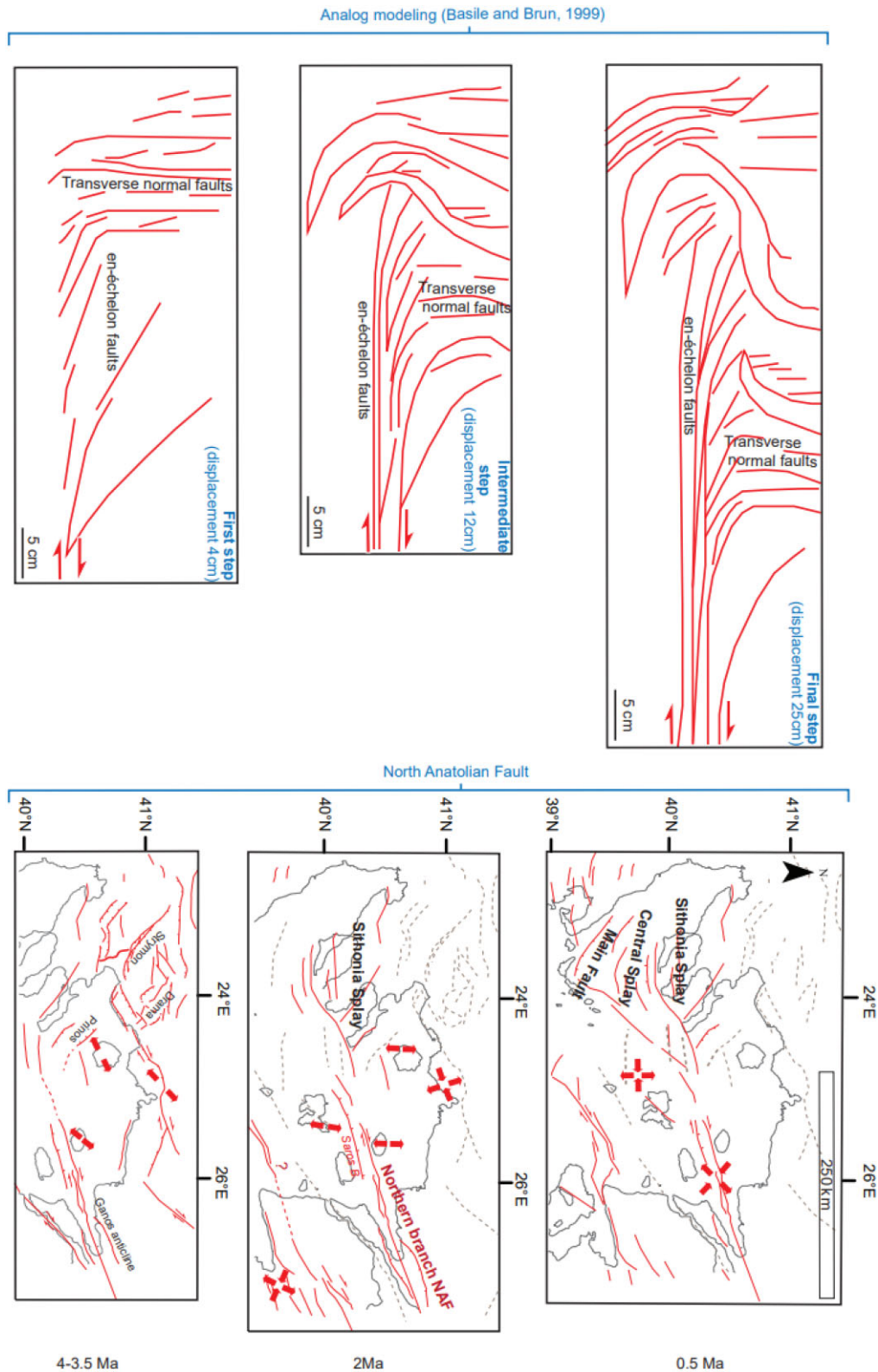


Figure 20. Analogue (sandbox) models for the evolution of horsetail termination, from Basile & Brun (1999), compared with the evolution of the North Aegean Trough horsetail (this study).

On the other hand, the North Aegean Trough consists in three horsetail basins (at the end of the Sithonia, Central and Main Splays) that merged in a single one. Our seismic data set highlights the successive activation of the Sithonia Splay at 2 Ma, the Central Splay

at 1.3 Ma and the Main Splay at 0.5 Ma, which corresponds to the westward propagation of the northern branch of the North Anatolian Fault (Fig. 18). The distance between the negative flower structure at the end of each splay is on the order of 30–50 km. This corresponds

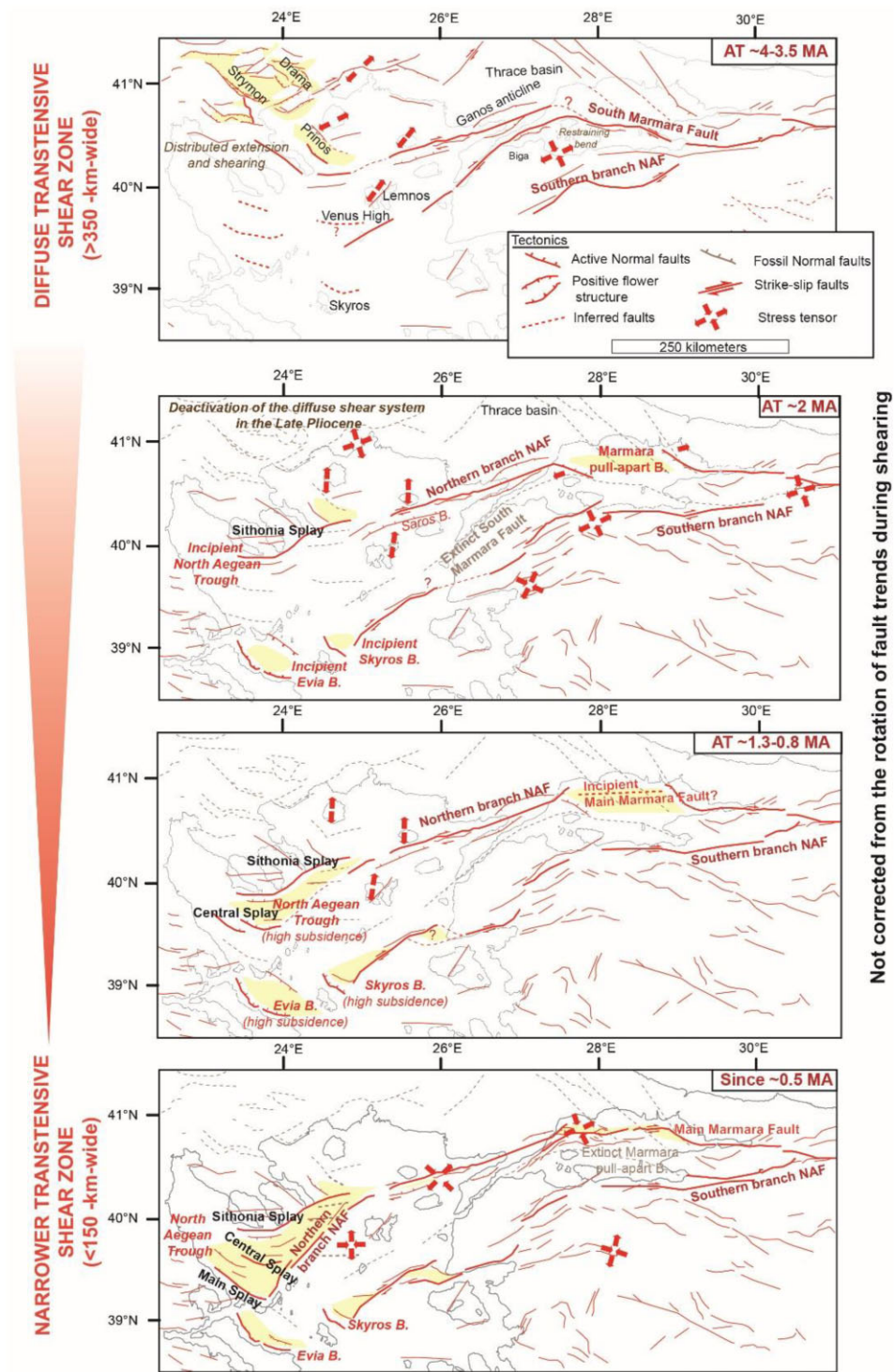


Figure 21. Structural evolution of the North Anatolian Fault in the North Aegean Domain, compiling field and offshore observations. This series of maps represents the present-day location of the faults that used to be active at 4–3.5 Ma, 2 Ma, 1.3–0.8 Ma and 0.5 Ma. The past shorelines are not reconstructed. Palaeo-stress tensors from Sümer *et al.* (2018) and Lybéris (1984).

to the distance added to the northern branch of the North Anatolian Fault every 0.7–0.8 Ma in the frame of its westward propagation. The three main splays of the North Aegean Trough have remained active since their inception. The decrease in slip rates observed in GPS measurements at the Sporadhes Archipelago (Müller *et al.*

2013) may be the result of slip partitioning over each major splay of the North Aegean Trough (Fig. 1).

This framework of structural evolution of the horsetail terminations encountered in the North Aegean Domain provides a ground-truth validation of analogue modelling tests performed by Basile

& Brun (1999). In their models (Fig. 20), a horsetail termination initially consists in an en-échelon normal fault system trending perpendicular to the main strike-slip displacement zone, composed of oblique Riedel splays. As the relative motion between the adjacent blocks increases, the Riedel splays progressively connects the en-échelon normal fault system. For dextral motion, the first Riedel fault forms to the east of the horsetail and the subsequent splays propagate westwards. Accordingly, the en-échelon normal faults are first captured in the overall horsetail structure in the east. The western en-échelon normal faults are progressively captured within the horsetail structure during its maturation. While some grabens associated to the en-échelon normal faults are captured by the oblique splays, others are crosscut by the propagating main displacement zone. Once initiated, all the oblique splays remain active during the lifetime of the horsetail.

6.2 The Plio-Pleistocene transition from a wide North Anatolian Shear Zone to a localized North Anatolian Fault

Our structural analysis further highlights the Late Pliocene change in stress regime (Lyberis 1984) at the scale of the North Aegean Domain (Fig. 21). From the Serravalian to the Late Pliocene, the North Anatolian Shear Zone consisted in a diffuse system of en-échelon normal faults connected through dextral transfer faults, thereby isolating a series of basins. These basins include a set of Late Miocene–Early Pliocene basins compartmentalizing the Rhodope Core complex (Brun & Sokoutis 2018) and the series of basins identified at sea in the vicinity of the North Aegean Trough, including the Athos and Venus grabens, deactivated at 2.8 Ma (Fig. 21a).

Our reconstructions at 2 and 1.3–0.8 Ma (Figs 21b and c) show the period of transition from the wide shear zone to the two main branches of the North Anatolian Fault; that is the period of effective propagation of the North Anatolian Fault in the North Aegean Sea. This transition is roughly coeval with the deactivation of the South Marmara Fault dated by Le Pichon *et al.* (2015) and the subsequent activation of the Main Marmara Fault. While propagating westward, the strike-slip segments of the North Anatolian Fault either connected or crosscut the Late Pliocene system of en-échelon grabens including the Athos and Venus grabens. Unconformity C (Figs 21c and d) records the first stage of formation of the northern and southern branches of the North Anatolian Fault at the North Aegean Trough and the Edremit-Skyros Trough, whereas unconformities B and A marks the successive steps of development of these basins.

If we consider the series of Serravalian–Pliocene basins dissecting the Rhodope Core complex (Brun & Sokoutis 2018) as the earliest traces of the North Anatolian Shear Zone in the North Aegean Domain, then the North Anatolian Shear Zone remained a diffuse transtensive system for about 5–7 Myr until the Messinian, with a first step of localization marked by the formation of the Ganos-Saros segment at ~5 Ma (Armijo *et al.* 1999). The Anatolia–Eurasia relative motion used to be distributed over this transtensive system composed of multiple en-échelon fault segments prior to Messinian. The enhanced localization of the North Anatolian Shear Zone in the North Aegean Domain evidenced here at 2–1.3 Ma coincides with the Early Pleistocene increase in slip-rates along the North Anatolian Fault (Hubert Ferrari *et al.* 2010). The localization of the North Anatolian Fault therefore contributed to the Early Pleistocene change in stress regime recorded over the entire Aegean, previously attributed to a change in the dynamics of the Hellenic Subduction

Zone (Lyberis 1984; Mascle & Martin 1990; Armijo *et al.* 1992; Sakellariou & Tsampouraki-Kraounaki 2016).

In this frame, the ‘wide shear-stage’ of the North Anatolian Shear Zone and the diachronous strain localization within it lasted several million years longer in the western North Aegean Domain than east of the Yeniçaga Fork (Fig. 21; Sengör *et al.* 2005). Some fault segments are localized since the Messinian (e.g. the Ganos-Saros fault) while others formed in the Early Pleistocene (e.g. the North Aegean and the Edremit-Skyros Troughs). This implies that some diffuse en-échelon systems (e.g. Chalkidiki or Marmara at 3.5–4 Ma) remain active while major, several hundred-km-long localized fault segments (e.g. Ganos-Saros segment) exist in between (Fig. 21). Further strain localization involved the abandonment of Late Miocene–Early Pliocene en-échelon faults (e.g. Strymon, Drama and Prinos) and major transfer strike-slip faults (e.g. transfer faults within the Thrace basin, the South Marmara Fault).

7 CONCLUSIONS

Our study documents multiple episodes of strain localization within the North Anatolian Shear Zone in the North Aegean Domain. During the Late Serravalian to the Early Pliocene, the North Anatolian Shear Zone was a diffuse transtensive fault zone. During the Late Pliocene, strike-slip strain localized along some fault segments (e.g. the Ganos-Saros segment) while remained diffuse in others (Prinos, Strymon, Drama, Thrace basins, Fig 21). Offshore sediments record the first abrupt step of strain localization along the northern and southern branches of the North Anatolian Fault in the North Aegean Domain at 2–1.3 Ma. This is coeval with the general increase of slip rate along the entire North Anatolian system and the regional change in stress regime over the Aegean Sea. Further westward propagation and localization along the northern and southern branches formed the North Aegean and Skyros-Edremit Troughs as horsetail structures. The North Aegean Trough results from the formation of three successive horsetails, formed at 2, 1.3 and 0.5 Ma and propagating westward at a rate of 40–60 km Myr⁻¹.

AUTHOR'S CONTRIBUTIONS

Conception of the project: M. Rodriguez; C. Gorini; D. Sakellariou; L. Lepourhiet; E. d'Acremont; S. Arsenikos; F. Chanier; P. Briole. *NAFAS cruise organization, Data acquisition and processing:* M. Rodriguez; A. Janin; E. d'Acremont; N. Chamot Rooke; K. Tsampouraki-Kraounaki; I. Morfis; G. Rousakis; A. Lurin; M. Delescluse; D. Oregioni; J.-X. Dessa; A. Necessian. *Multibeam acquisition and interpretation:* D. Sakellariou; I. Morfis; G. Rousakis; K. Tsampouraki Karounaki; M. Rodriguez. *Seismic interpretation:* M. Rodriguez; A. Janin; A. Lurin; C. Gorini; D. Sakellariou. *Geological expertise, integration of the results to the geological background:* M. Rodriguez; D. Sakellariou; C. Gorini; P. Henry; C. Grall; A. Beniést; D. Fernandez Blanco; A. Rigo; C. Bulois; F. Chanier; F. Caroir; L. Lepourhiet.

ACKNOWLEDGMENTS

We warmly thank the crew members of the R/V Tethys II involved in the NAFAS cruise. This study benefits from the support of INSU,CNRS (RHEOSTRIKE project). We warmly thank L. Jolivet and M. Laigle for their precious support and helpful advices. We thank Dr Vasiliki Mouslopoulou and an anonymous reviewer for their highly constructive and helpful comments. We dedicate

this study to the memory of Prof Jean-Pierre Brun, who supported and inspired us during the earliest stages of this project.

CONFLICT OF INTEREST

The authors do not have any conflict of interest.

DATA AVAILABILITY

Seismic reflexion data set available on request to Dr M. Rodriguez (rodriguez@geologie.ens.fr) and Dr M. Delescluse (delescluse@geologie.ens.fr).

Multibeam data set available on emodnet <https://emodnet.ec.europa.eu/en/bathymetry>

References

- Anastasakis, G. & Piper, D.J.W., 2005. Late Neogene evolution of the western South Aegean volcanic arc: sedimentary imprint of volcanicity around Milos, *Mar. Geol.*, **215**, 135–158.
- Anastasakis, G. & Piper, D.J.W., 2013. The changing architecture of sea-level lowstand deposits across the Mid-Pleistocene transition: south Evoikos Gulf, Greece, *Quat. Sci. Rev.*, **73**, 103–114.
- Anastasakis, G., Piper, D.J.W., Dermitzakis, M.D. & Karakitsios, V., 2006. Upper Cenozoic stratigraphy and paleogeographic evolution of Myrtoon and adjacent basins, Aegean Sea, Greece, *Mar. Pet. Geol.*, **23**, 353–369.
- Armijo, R., Lyon-Caen, H. & Papanastassiou, D., 1992. East-west extension and Holocene normal-fault scarps in the Hellenic arc, *Geology*, **20**, 491–494.
- Armijo, R., Meyer, B., Hubert, A. & Barka, A., 1999. Westward propagation of the North Anatolian fault into the northern Aegean: timing and kinematics, *Geology*, **27**, 267–270.
- Basile, C. & Brun, J.-P., 1999. Transtensional faulting patterns ranging from pull-apart basins to transform continental margins: an experimental investigation, *J. Struct. Geol.*, **21**, 23–37.
- Beniest, A., Brun, J.-P., Gorini, C., Crombez, V., Deschamps, R., Hamon, Y. & Smit, J., 2016. Interaction between trench retreat and anatolian escape as recorded by neogene basins in the northern Aegean Sea, *Mar. Petrol. Geol.*, **77**, 30–42.
- Ben-Zion, Y. & Sammis, C.G., 2003. Characterization of fault zones, *Pure appl. Geophys.*, **160**, 677–715.
- Brooks, M. & Ferentinos, G., 1980. Structure and evolution of the Sporadhes basin of the North Aegean trough, northern Aegean Sea, *Tectonophysics*, **68**, 15–30.
- Brun, J.-P. & Faccenna, C., 2008. Exhumation of high-pressure rocks driven by slab rollback, *Earth planet. Sci. Lett.*, **272**, 1–7.
- Brun, J.-P., Faccenna, C., Gueydan, F., Sokoutis, D., Philippon, M., Kydonakis, K. & Gorini, C., 2016. The two-stage Aegean extension, from localized to distributed, a result of slab rollback acceleration, *Can. J. Earth Sci.*, **53**, 1142–1157.
- Brun, J.-P. & Sokoutis, D., 2018. Core complex segmentation in North Aegean, a dynamic view, *Tectonics*, **37**, 1797–1830.
- Bulut, F., Özener, H., Dogru, A., Aktug, B. & Yaltrak, C., 2018. Structural setting along the Western North Anatolian Fault and its influence on the 2014 North Aegean Earthquake (Mw 6.9), *Tectonophysics*, **745**, 382–394.
- Calvo, J.P., Triantaphyllou, M.V., Regueiro, M. & Stamatakis, M.G., 2012. Alternating diatomaceous and volcanoclastic deposits in Milos Island, Greece. A contribution to the upper Pliocene-lower Pleistocene stratigraphy of the Aegean Sea, *Palaeogeograph., Palaeoclimatol., Palaeoecol.*, **321–322**, 24–40.
- Carton, H. *et al.* 2007. Seismic imaging of the three-dimensional architecture of the Cinarcik basin along the North Anatolian Fault, *J. geophys. Res.*, **112**(B6), doi:10.1029/2006JB004548.
- Chamot-Rooke, N. *et al.*, 2005. *Deep Offshore Tectonics of the Eastern Mediterranean: A Synthesis of Deep Marine Data in the Eastern Mediterranean: The Ionian Basin and Margins, the Calabria Wedge and the Mediterranean Ridge, Mémoires de la Société Géologique de France: Société Géologique de France* Issue 177 of *Mémoires de la Société géologique de France*, ISSN 0249-7549, Société géologique de France.
- Collier, R.E.L. & Dart, C.J., 1991. Neogene to Quaternary rifting, sedimentation and uplift in the Corinth Basin, Greece, *J. Geol. Soc. Lond.*, **148**(6), 1049–1065.
- Demoulin, A., Altin, T.B. & Beckers, A., 2013. Morphometric age estimate of the last phase of accelerated uplift in the Kazdag area (Biga Peninsula, NW Turkey), *Tectonophysics*, **608**, 1380–1393.
- Dietrich, V.J., Mercolli, I. & Oberhänsli, R., 1988. Dazite, High-Alumina Basalte und Andesite als Produkte amphiboldomierter Differentiation (Aegina und Methan, Agaischer Inselbogen), *Schweizische Mineralogische und Petrographische Mitteilungen*, **68**, 21–39.
- Dooley, T. & Schreurs, G., 2012. Analogue modelling of intraplate strike-slip tectonics: a review and new experimental results. *Tectonophysics*, **574–575**, 1–71.
- Endrun, B., Lebedev, S., Meier, T., Tirel, C. & Friederich, W., 2011. Complex layered deformation within the Aegean crust and mantle revealed by seismic anisotropy, *Nat. Geosci.*, **4**, 203–207.
- England, P., Houseman, G. & Nocquet, J.-M., 2016. Constraints from GPS measurements on the dynamics of deformation in Anatolia and the Aegean. *J. geophys. Res.*, **121**, 8888–8916.
- Faccenna, C., Bellier, O., Martinod, J., Piromallo, C. & Regard, V., 2006. Slab detachment beneath eastern Anatolia: a possible cause for the formation of the North Anatolian fault, *Earth Planet. Sci. Lett.*, **242**, 85–97.
- Faugères, J.C., Gonthier, E., Mulder, T., Kenyon, N., Cirac, P., Griboulaud, R., Berné, S. & Lesuavé, R., 2002. Multiprocess generated sediment waves on the Landes Plateau (Bay of Biscay, North Atlantic), *Mar. Geol.*, **182**, 279–302.
- Ferentinos, G., Georgiou, N., Christodoulou, D., Geraga, M. & Papatheodorou, G., 2018. Propagation and termination of a strike slip fault in an extensional domain: the westward growth of the North Anatolian Fault into the Aegean Sea, *Tectonophysics*, **745**, 183–195.
- Flerit, F., Armijo, R., King, G. & Meyer, B., 2004. The mechanical interaction between the propagating North Anatolian Fault and the back-arc extension in the Aegean, *Earth planet. Sci. Lett.*, **224**, 347–362.
- Floyd, M.A. *et al.*, 2010. A new velocity field for Greece: implications for the kinematics and dynamics of the Aegean, *J. geophys. Res.*, **115**(B10), doi:10.1029/2009JB007040.
- Ford, M., Rohais, S., Williams, E.A., Bourlange, S., Jousset, D., Backert, N. & Malartre, F., 2013. Tectono-sedimentary evolution of the western Corinth rift (Central Greece), *Basin Res.*, **25**, 3–25.
- Fytikas, M., Giuliani, O., Innocenti, F., Marinelli, G. & Mazzuoli, R., 1976. Geochronological data on recent magmatism of the Aegean Sea, *Tectonophysics*, **31**, T29–T34.
- Fytikas, M., Innocenti, F., Kolios, N., Manetti, P., Mazzuoli, R., Poli, G., Rita, F. & Villari, L., 1986. Volcanology and petrology of volcanic products from the island of Milos and neighbouring islets, *J. Volc. Geotherm. Res.*, **28**, 297–317.
- Garfunkel, Z. & Ben-Avraham, Z., 1996. The structure of the Dead Sea basin, *Tectonophysics*, **266**, 155–176.
- Grall, C. *et al.* 2013. Slip rate estimation along the western segment of the Main Marmara Fault over the last 405–490 ka by correlating mass transport deposits, *Tectonics*, **32**, 1587–1601.
- Grall, C., Henry, P., Tezcan, D., Géli, L., de Lépina, B.-M., Rudkiewicz, J.-L., Zitter, T. & Harmegnies, F., 2012. Heat flow in the Sea of Marmara Central Basin: possible implications for the tectonic evolution of the North Anatolian Fault, *Geology*, **40**, 3–6.
- Gürer, Ö., Sangu, E., Özbüran, M., Gürbüz, A., Gürer, A. & Simir, H., 2016. Plio-Quaternary kinematic development and paleostress pattern of the Edremit Basin, Western Turkey, *Tectonophysics*, **679**, 199–210.
- Handy, M.R., Schmid, S.M., Bousquet, R., Kissling, E. & Bernoulli, D., 2010. Reconciling plate-tectonic reconstructions of Alpine Tethys with the geological-geophysical record of spreading and subduction in the Alps, *Earth Sci. Rev.*, **102**, 121–158.

- Hébert, H., Schindele, F., Altinok, Y., Alpar, B. & Gazioglu, C., 2005. Tsunami hazard in the Marmara Sea (Turkey): a numerical approach to discuss active faulting and impact on the Istanbul coastal areas, *Mar. Geol.*, **215**, 23–43.
- Hsu, K.J. et al. 1978. Site 378, Cretan Basin, *Init Rep. DSDP*, **42**, 321–357.
- Hubert-Ferrari, A., Barka, A., Jacques, E., Nalbant, S.S., Meyer, B., Armijo, R., Tapponnier, P. & King, G.C.P., 2000. Seismic hazard in the Marmara Sea region following the 17 August 1999 Izmit earthquake, *Nature*, **404**, 269–273.
- Hubert Ferrari, A., King, G., Van der Woerd, J., Villa, I., Altunel, E. & Armijo, R., 2010. Long-term evolution of the North Anatolian Fault: new constraints from its eastern termination, *Geol. Soc. Lond., Spec. Pub.*, **311**(1), 133–154.
- Islamoglu, Y., Harzhauser, M., Gross, M., Jimenez-Moreno, G., Coric, S., Kroh, A., Rögl, F. & van der Made, J., 2008. From Tethys to eastern Paratethys: oligocene depositional environments, paleoecology and paleobiogeography of the Thrace Basin (NW Turkey), *Int. J. Earth Sci.*, **18**, 183–200.
- Isler, E., Aksu, A., Yaltrak, C. & Hiscott, R., 2008. Seismic stratigraphy and Quaternary sedimentary history of the northeast Aegean Sea, *Mar. Geol.*, **254**, 1–17.
- Janin, A., Rodriguez, M., Sakellariou, D., Lykousis, V. & Gorini, C., 2019. Tsunamigenic potential of a Holocene submarine landslide along the North Anatolian Fault (northern Aegean Sea, off Thasos island): insights from numerical modelling, *Nat. Haz. Earth Syst. Sci.*, **19**, 121–136.
- Jolivet, L. et al. 2013. Aegean tectonics: strain localisation, slab tearing and trench retreat, *Tectonophysics*, **597–598**, 1–33.
- Jolivet, L. et al. 2015. The geological signature of a slab tear below the Aegean, *Tectonophysics*, **659**, 166–182.
- Jolivet, L. et al. 2021. Transfer zones in Mediterranean back-arc regions and tear faults, *Bull. Soc. Géol. France*, **192**(1), doi:10.1051/bsgf/2021006.
- Jolivet, L. & Brun, J.-P., 2010. Cenozoic geodynamic evolution of the Aegean, *Int. J. Earth Sci.*, **99**, 109–138.
- Jolivet, L. & Faccenna, C., 2000. Mediterranean extension and the Africa-Eurasia collision, *Tectonics*, **19**, 1095–1106.
- Karakas, C., Armijo, R., Lacassin, R., Suc, J.-P. & Melinte-Drobinescu, M.C., 2018. Crustal strain in the Marmara pull-apart region associated with the propagation process of the North Anatolian Fault, *Tectonics*, **37**, 1507–1523.
- Karakitsios, V. et al. 2017. Messinian salinity crisis record under strong freshwater input in marginal, intermediate, and deep environments: the case of the North Aegean, *Palaeogeogr. Palaeoclimatol. Palaeoecol.*, **485**, 316–335.
- Kiratzi, A. & Louvari, E., 2003. Focal mechanisms of shallow earthquakes in the Aegean Sea and the surrounding lands determined by waveform modelling: a new database, *J. Geodyn.*, **36**, 251–274.
- Konstantinou, K.I., Mouslopoulou, V., Liang, W.-T., Heidbach, O., Oncken, O. & Suppe, J., 2017. Present-day crustal stress field in Greece inferred from regional-scale damped inversion of earthquake focal mechanisms, *J. geophys. Res.*, **122**, 506–523.
- Koukouvelas, I.K. & Aydin, A., 2002. Fault structure and related basins of the North Aegean Sea and its surroundings, *Tectonics*, **21**, 10–11-10-17.
- Kourouklas, C., Tsaklidis, G., Papadimitriou, E. & Karakostas, V., 2022. Analyzing the correlations and the statistical distribution of moderate to large earthquakes interevent times in Greece, *Appl. Sci.*, **12**, doi:10.3390/app12147041.
- Kreemer, C. & Chamot-Rooke, N., 2004. Contemporary kinematics of the Southern Aegean and the Mediterranean Ridge, *Geophys. J. Int.*, **157**, 1377–1392.
- Krijgsman, W. et al., 2022. Mediterranean-Black Sea gateway exchange: scientific drilling workshop on the BlackGate project, *Sci. Dril.*, **31**, 93–110.
- Lafosse, M. et al. 2020. Plio-Quaternary tectonic evolution of the southern margin of the Alboran Basin (Western Mediterranean), *Solid Earth*, **11**, 741–765.
- Laigle, M., Hirn, A., Sachpazi, M. & Roussos, N., 2000. North Aegean crustal deformation: an active fault imaged to 10 km depth by reflection seismic data, *Geology*, **28**, 71–74.
- Lefevre, M., Souloumiac, P., Cubas, N. & Klinger, Y., 2020. Experimental evidence for crustal control over seismic fault segmentation, *Geology*, **48**, 844–848.
- Le Pichon, X. et al. 2001. The active main Marmara fault, *Earth planet. Sci. Lett.*, **192**, 595–616.
- Le Pichon, X., Chamot-Rooke, N. & Rangin, C., 2003. The North Anatolian fault in the Sea of Marmara, *J. geophys. Res.*, **108**, 2179.
- Le Pichon, X., Imren, C., Rangin, C., Sengör, A.M.C. & Siyako, M., 2014. The South Marmara Fault, *Int. J. Earth Sci.*, **103**, 219–231.
- Le Pichon, X., Sengör, A.M.C., Kende, J., Imren, C., Henry, P., Grall, C. & Karabulut, H., 2015. Propagation of a strike-slip plate boundary within an extensional environment: the westward propagation of the North Anatolian Fault, *Can. J. Earth Sci.*, **53**, 1416–1439.
- Le Pichon, X. & Kreemer, C., 2010. The Miocene-to-present kinematic evolution of the eastern Mediterranean and Middle East and its implications for dynamics, *Annu. Rev. Earth planet. Sci.*, **38**, 323–351.
- Le Pourhiet, L., Huet, B., May, D.A., Labrousse, L. & Jolivet, L., 2012. Kinematic interpretation of the 3D shapes of metamorphic core complexes, *Geochem. Geophys. Geosyst.*, **13**(9), doi:10.1029/2012GC004271.
- Le Pourhiet, L., Huet, B. & Traoré, N., 2014. Links between long-term and short-term rheology of the lithosphere: insights from strike-slip fault modelling, *Tectonophysics*, **631**, 146–159.
- Lyberis, N., 1984. Tectonic evolution of the North Aegean trough, *Geol. Soc. London Spec. Publ.*, **17**, 709–725.
- Lykousis, V., 2009. Sea-level changes and shelf break prograding sequences during the last 400 ka in the Aegean margins: subsidence rates and palaeogeographic implications, *Cont. Shelf Res.*, **29**, 2037–2044.
- Lykousis, V., Roussakis, G., Alexandri, M., Pavlakis, P. & Papoulia, I., 2002. Sliding and regional slope stability in active margins: north Aegean Trough (Mediterranean), *Mar. Geol.*, **186**, 281–298.
- Mann, P., 2007. Global catalogue, classification and tectonic origins of restraining- and releasing bends on active and ancient strike-slip fault systems, *Geol. Soc. Lond., Spec. Publ.*, **290**, 13–142.
- Mascle, J. & Martin, L., 1990. Shallow structure and recent evolution of the Aegean Sea: a synthesis based on continuous reflection profiles. *Mar. Geol.*, **94**, 271–299.
- McNeill, L.C., Mille, A., Minshull, T.A., Bull, J.M. & Kenyon, N.H., 2004. Extension of the North Anatolian Fault into the North Aegean Trough: evidence for transtension, strain partitioning, and analogues for Sea of Marmara basin models, *Tectonics*, **23**(2), doi:10.1029/2002TC001490.
- Melinte-Drobinescu, M.C. et al. 2009. The messinian salinity crisis in the dardanelles region: chronostratigraphic constraints, *Palaeogeogr. Palaeoclimatol. Palaeoecol.*, **278**, 24–39.
- Mouslopoulou, V., Nicol, A., Little, T.A. & Walsh, J.J., 2007a. Terminations of large strike-slip faults: an alternative model from New Zealand, in *Tectonics of Strike-Slip Restraining and Releasing Bends*, Vol. **290**, pp. 387–415, eds Cunningham, W.D. & Mann, P., Geological Society of London, Special Publication.
- Müller, M.D., Geiger, A., Kahle, H.-G., Veis, G., Billiris, H., Paradissis, D. & Felekis, S., 2013. Velocity and deformation fields in the North Aegean domain, Greece, and implications for fault kinematics, derived from GPS data 1993–2009, *Tectonophysics*, **597–598**, 34–49.
- Nixon, C.W. et al., 2016. Rapid spatiotemporal variations in rift structure during development of the Corinth Rift, central Greece, *Tectonics*, **35**, 1225–1248.
- Okay, A.I. & Tüysüz, O., 1999. Tethyan sutures of northern Turkey, *Geol. Soc. Lond., Spec. Pub.*, **156**, 475–515.
- Papanikolaou, D., Alexandri, M., Nomikou, P. & Ballas, D., 2002. Morpho-tectonic structure of the western part of the North Aegean Basin based on swath bathymetry, *Mar. Geol.*, **190**, 465–492.
- Papanikolaou, D., Nomikou, P., Papanikolaou, I., Lampridou, D., Rousakis, G. & Alexandri, M., 2019. Active tectonics and seismic hazard in Skyros Basin, North Aegean Sea, Greece, *Mar. Geol.*, **407**, 94–110.
- Papatheodorou, G., Hasiotis, T. & Ferentinos, G., 1993. Gas-charged sediments in the Aegean and Ionian Seas, Greece, *Mar. Geol.*, **112**, 171–184.
- Pe-Piper, G., Piper, D.J.W. & Reynolds, P.H., 1983. Paleomagnetic stratigraphy and radiometric dating of the Pliocene volcanic rocks of Aegina, Greece, *Bull. Volcanol.*, **46**, 1–7.

- Perouse, E., Chamot-Rooke, N., Rabaute, A., Briole, P., Jouanne, F., Georgiev, I. & Dimitrov, D., 2012. Bridging onshore and offshore present-day kinematics of central and eastern Mediterranean: implications for crustal dynamics and mantle flow, *Geochem. Geophys. Geosyst.*, **13**(9), doi:10.1029/2012gc004289.
- Piper, D.J. & Perissoratis, C., 1991. Late Quaternary Sedimentation on the North Aegean Continental Margin, Greece, *AAPG Bull.*, **75**, 46–61.
- Porkoláb, K., Willingshofer, E., Sokoutis, D., Békési, E. & Beekman, F., 2023. Post-5 Ma rock deformation on Alonnisos (Greece) constrains the propagation of the North Anatolian Fault, *Tectonophysics*, **846**, doi:10.1016/j.tecto.2022.229654.
- Proedrou, P. & Papaconstantinou, C.M., 2004. Prinos basin – a model for oil exploration, *Bull. Geol. Soc. Greece*, **36**, 327–333.
- Proedrou, P. & Sidiropoulos, T., 1992. Prinos field-Greece, Aegean basin, structural traps, in *Treatise of Petroleum Geology Atlas of Oil and Gas Fields*, pp. 275–291, AAPG.
- Rangin, C., Le Pichon, X., Demirbag, E. & Imren, C., 2004. Strain localization in the Sea of Marmara: propagation of the North Anatolian Fault in a now inactive pull-apart, *Tectonics*, **23**(2), doi:10.1029/2002TC001437.
- Rebesco, M., Hernández-Molina, F.J., Van Rooij, D. & Wahlin, A., 2014. Contourites and associated sediments controlled by deep-water circulation processes: state of the art and future considerations, *Mar. Geol.*, **352**, 111–154.
- Reicherter, K., Papanikolaou, I., Roger, J., Mathes-Schmidt, M., Papanikolaou, D., Rössler, S., Grützner, C. & Stamatis, G., 2010. Holocene tsunamigenic sediments and tsunami modelling in the Thermaikos Gulf area (northern Greece), *Zeitschrift für Geomorphol. Suppl. Issues*, **54**, 99–125.
- Reilinger, R. *et al.*, 2006. GPS constraints on continental deformation in the Africa–Arabia–Eurasia continental collision zone and implications for the dynamics of plate interactions, *J. geophys. Res.*, **111**(B5), doi:10.1029/2005JB004051.
- Rodríguez, M. *et al.* 2018. Seismic profiles across the North Anatolian Fault in the Aegean Sea, in *EGU General Assembly Conference Abstracts*, Vol. **20**, EGU2018-7426, AGU.
- Roussos, N. & Lyssimachou, T., 1991. Structure of the Central North Aegean trough: an active strike-slip deformation zone, *Basin Res.*, **3**, 37–46.
- Sakellariou, D. *et al.* 2018. Deformation and kinematics at the termination of the North Anatolian Fault: the North Aegean Trough horseshoe structure, in *Proceedings of the 9th International INQUA Meeting on Paleoseismology, Active Tectonics and Archeoseismology (PATA)*, 25–27 June 2018, Possidi, Greece, pp. 237–240.
- Sakellariou, D. & Galanidou, N., 2017. Aegean Pleistocene landscapes above and below sea-level: Palaeogeographic reconstruction and Hominin dispersals, in *Under the Sea: Archaeology and Palaeolandscapes of the Continental Shelf*, Coastal research library, Vol. 20, pp. 335–359, eds Bailey, G., Harff, J. & Sakellariou, D., Springer.
- Sakellariou, D. & Tsampouraki-Kraounaki, K., 2016. Offshore faulting in the Aegean Sea: a synthesis based on bathymetric and seismic profiling data, *Bull. Geol. Soc. Greece*, **50**, 124–133.
- Sakellariou, D. & Tsampouraki-Kraounaki, K., 2018. Plio-Quaternary extension and strike-slip tectonics in the Aegean, in *Transform Plate Boundaries and Fracture Zones*, Chapter 14, pp. 339–374, ed. Duarte, J., Elsevier.
- Schettino, A. & Turco, E., 2011. Tectonic history of the western Tethys since the Late Triassic, *GSA Bull.*, **123**, 89–105.
- Sengör, A.M.C., Grall, C., Imren, C., LePichon, X., Görür, N., Henry, P., Karabulut, H. & Siyako, M., 2014. The geometry of the North Anatolian transform fault in the Sea of Marmara and its temporal evolution: implications for the development of intracontinental transform faults, *Can. J. Earth Sci.*, **51**, 222–242.
- Sengör, A.M.C., Tüysüz, O., Imren, C., Sakinc, M., Eyidogan, H., Görür, N., LePichon, X. & Rangin, C., 2005. The North Anatolian fault: a new look, *Annu. Rev. Earth planet. Sci.*, **33**(1), 37–112.
- Sengör, A.M.C., Zabcı, C. & Nata'ın, B.A., 2019. Continental transform faults: congruence and incongruence with normal plate kinematics, in *Transform Plate Boundaries and Fracture Zones*, pp. 170–246, ed. Duarte, J., Elsevier.
- Shillington, D.J. *et al.* 2012. Evidence of widespread creep on the flanks of the Sea of Marmara transform basin from marine geophysical data, *Geology*, **40**, 439–442.
- Siyako, M. & Huvaz, O., 2007. Eocene stratigraphic evolution of the Thrace Basin, *Turk. Sediment. Geol.*, **198**, 75–91.
- Sodoudi, F. *et al.* 2006. Lithospheric structure of the Aegean obtained from P and S receiver functions, *J. geophys. Res.*, **111**(B12), doi:10.1029/2005JB003932.
- Suc, J.-P. *et al.* 2015. Marine gateway vs. fluvial stream within the Balkans from 6 to 5 Ma, *Mar. Petrol. Geol.*, **66**, 231–245.
- Sümer, Ö., Uzel, B., Özkaymak, C. & Sözbilir, H., 2018. Kinematics of the Havran-Balıkesir Fault Zone and its implication on geodynamic evolution of the Southern Marmara Region, NW Anatolia, *Geodin. Acta*, **30**, 306–323.
- Tchalenko, J.S., 1970. Similarities between shear zones of different magnitudes, *Geol. Soc. Am. Bull.*, **81**, 1625–1640.
- Tchalenko, J.S. & Ambraseys, N.N., 1970. Structural analysis of the Dasht-e Bayaz (Iran) earthquake fractures, *Geol. Soc. Am. Bull.*, **81**, 41–60.
- Tripanas, E.K., Panagiotopoulos, I.P., Lykousis, V., Morfis, I., Karageorgis, A.P., Anastakis, G. & Kontogonis, G., 2016. Late quaternary bottom-current activity in the south Aegean Sea reflecting climate-driven dense-water production, *Mar. Geol.*, **375**, 99–119.
- Turgut, S. & Eseller, G., 2000. Sequence stratigraphy, tectonics and depositional history in eastern Thrace Basin, NW Turkey, *Mar. Petrol. Geol.*, **17**, 61–100.
- Varesis, A. & Anastakis, G., 2021. Cenozoic marine basin evolution in the western North Aegean Trough margin: seismic stratigraphic evidence, *Water*, **13**(16), doi:10.3390/w13162267.
- Wesnousky, S.G., 2005. The San Andreas and Walker Lane fault systems, western North America: transpression, transtension, cumulative slip and the structural evolution of a major transform plate boundary, *J. Struct. Geol.*, **27**, 1505–1512.
- Woodcock, N.H. & Daly, M.C., 1986. The role of strike-slip fault systems at plate boundaries, *Phil. Trans. R. Soc. A*, **317**, 13–29.
- Yalçın, H., Kürçer, A., Utku, M. & Gülen, L., 2016. Seismotectonics of the Southern Marmara region, NW Turkey, *Bull. Geol. Soc. Greece*, **50**, 173–181.
- Anastasakis, G. & Piper, D.J.W. 2013. The changing architecture of sea-level lowstand deposits across the Mid-Pleistocene transition: South Evoikos Gulf, Greece, *Quaternary Science Reviews*, **73**, 103–114.